國立交通大學

理學院 應用化學系

碩士論文

Department of Applied Chemistry, College of Science

National Chiao Tung University

Development of Mass Spectrometric Methods for the Monitoring of Biocatalytic Processes

發展用於監測動態生物催化反應之質譜分析方法

研 究 生： 丁 煦　　Student: Hsu Ting

指導教授： 帕偉鄂本 博士　　Advisor: Dr Pawel L. Urban

中 華 民 國 103 年 6 月

June, 2014

Development of Mass Spectrometric Methods for the Monitoring of Biocatalytic Processes

發展用於監測動態生物催化反應之質譜分析方法

研 究 生： 丁 煦　　Student: Hsu Ting

指導教授： 帕偉鄂本 博士　　Advisor: Dr Pawel L. Urban

國立交通大學

理學院 應用化學系

碩士論文

A thesis submitted to M. S. Program,
Department of Applied Chemistry
College of Science,
National Chiao Tung University,
in partial fulfillment of the requirements
for the Degree of Master of Science
in Applied Chemistry

June, 2014

Hsinchu, Taiwan

中華民國一百零三年六月

中文摘要

在生物催化反應中，酵素的參與可使化學反應在有限的時間內加速生成並且增加產率。酵素在細胞及生物流體中無所不在，並且於所有的代謝過程中有著重要的地位. 而它們也被運用在工業合成各式化學品及生物燃料等。在學術界或是工業用途中，為了研究或使用酵素的催化能力，找到適合的分析方法對酵素系統進行化學性質分析是重要且需要的。質譜技術能夠偵測分析物在時間中的變化，對分析物有相當高的特異性；對於監測酵素反應系統的過程相當重要，所以質譜技術在這份論文中可作為一個理想的偵測工具。在第一部分的研究中，我開發了一個質譜分析方法對於假設的化學訊號傳導現象做探討與解釋，此反應中使用的兩種酵素分別為肌激酶和丙酮酸激酶。藉由大氣壓力游離法的配置，呈現在一高長寬比的液體區間中，化學波的傳遞速度超越如對流與擴散等自然傳輸所造成的現象。而當使用同位素標記的受質當作啟動催化的反應物時，可以同時展現及監測到兩種類型的化學傳遞。在第二部分的研究中，我開發了一個自製的自動化設備，包含了開放式資源的電子操作裝置和數個低成本的機械配備，用於監測固定化之脂解酶對轉酯化反應之催化。整套裝置的運行由一套使用 Linux 系統以及輸入 C 程式語言的單板機微電腦所操控。由於技術上的改進，在一小體積反應腔中隨著時間變化的樣品可以被自動注射至氣相層析質譜儀做分析。這套裝置可以用來監測由單一顆粒(< 1 毫米)固定化脂解酶所催化之反應，而這類固態生物催化劑擁有的催化異質性展現於分析結果。此外，這個分析方法也能夠使用於監測植物組織在液相萃取中的動態過程。在此研究中，轉酯化反應中的產物 - 乙酸正丁酯與在植物組織中出現的三種萜類運用此法完成了定量分析。R^2 的值在 0.944-0.989 之間，而偵測極限則是在亞微莫耳之間。簡而言之，兩種不同的質譜分析法分別已被建立，一可用於觀察藉由酵素反應隨者時間與空間所產生之傳輸變化，另一可用於監測工業應用有關的酵素催化反應隨時間所產生的動態變化。

Abstract

Biocatalysis encompasses the use of enzymes to speed up chemical reactions thus increasing reaction yields within limited time periods. Enzymes are omnipresent. They are involved in all metabolic processes occurring in cells and biofluids. They also find applications in industry, in the synthesis of fine chemicals and biofuels. In order to utilize the catalyzing ability of enzymes in academic research or industry, suitable analytical methods are required to determine their activities. Mass spectrometry is an ideal tool for monitoring the progress of enzymatic processes because it allows one to follow temporal concentration profiles of reactants while ascertaining high specificity. In the first part of the project, I developed a mass spectrometric method to demonstrate a hypothesized phenomenon of chemical signal transduction aided by a set of two enzymes: adenylate kinase and pyruvate kinase. By implementing an atmospheric pressure ionization technique, it was possible to obtain spatiotemporal characteristics of chemical wave propagating in a high-aspect-ratio volume of liquid with a speed exceeding that of natural processes such as convection and diffusion. By using an isotopically labeled substrate ($^{13}C_{10}$ adenosine triphosphate) as the triggering reagent, the two types of chemical propagation could be revealed and monitored simultaneously. In the second part of the project, I implemented a home-built automated setup – incorporating open-source electronic control unit and a number of inexpensive actuators – to monitor transesterification catalyzed by immobilized lipase. The analysis was guided by a program in C language, deployed on a single-board Linux-based microcomputer. Thanks to this technological improvement, the temporal samples, collected from a low-volume reaction chamber, were automatically injected to the gas chromatography – mass spectrometry apparatus. The proposed system enabled monitoring reactions catalyzed by single microbeads (< 1 mm) of immobilized lipase, and drawing conclusions on catalytic heterogeneity of this solid-state biocatalyst. Furthermore, it allowed one to monitor the progress of liquid extraction of fresh plant tissue. Quantitative analysis of 1-butyl acetate formed in the course of transesterification, and three terpenes – extracted from plant tissue – was achieved. The R^2 of the calibration plot was in the range 0.944 – 0.989, and the limits of detection of the target compounds were in the submicromolar range. In summary, two methods have been developed which can assist observation of spatiotemporal phenomena involving enzymes, and temporal screening of dynamic processes relevant to industrial applications.

誌　謝

在最後的最後，總算踏入了碩士生涯的終點站，兩年的時間不算長也不算短，但總歸是一條必經之路。初來乍到新竹的時候，看著學長們為畢業忙的焦頭爛額，現在終於了解他們的感受。我也從一個不知所云的碩士菜鳥，逐漸地學會獨立和自主學習，並且在時間管理與分配上有著明顯的改善，可能是因為事情比較多吧! 一路走來或許不是很順遂，但是也因為如此，我獲得的更多! 感謝我的指導老師帕偉鄂本教授，他對科學的嚴謹以及耐心的教學使我受益匪淺，使自己的實驗能夠順利地進行進而得到不錯的成果；此外，在英文聽說方面也有了十足的長進! 也非常感謝陳月枝教授與余艇教授在口試時給予的指點與幫助，對於論文的完成度與完整性有著顯著的提升，也讓我有機會從不同角度審視自己的研究。

再來是實驗室的同仁們，因為有你們的包容及支持，我才能開心地度過這一個研究生生涯。傑筆、杜伊玲、凱達、士豪、思穎、佑青，不管是跟你們討論實驗，運動或是到處亂吃，話匣子打開就可以聊到昏天暗地!謝謝你們的陪伴，完美了我的最後兩年學生生活，亭汝跟雅洳雖然我們只有認識短短的一個月，但是我相信你們可以相處得很愉快。在新竹沒事一起打屁吃飯的弘盛跟凱哥，中山的殷孝，中興的嘟嘟，許老師家的子胤、丁丁、書豪、佳容，裘老師家的毓翔，陳老師家的西哥，還有昱良、阿龍、志偉、富為、金吉還有李柏等學長們的照顧。因為有大家的支持與愛護，我才可以存活下來。

最後，我想感謝一個對我來說很重要的人－Andrea Chiu，如果沒有她，我可能也沒這個機會攻讀碩士；在我得意的時候，她提醒我要謙虛；我失落的時候，她鼓勵我不要氣餒，謝謝她在我背後默默的付出和支持，讓我沒有後顧之憂地往前邁進。期許自己變得更好，換我當妳的依靠。謝謝妳的家人也對我相當的照顧! 希望大家都可以逐步實現自己的目標，勇敢追夢! 請讓我分享這份喜悅給你們，再一次謝謝所有幫助過我的人，後會有期!

Table of contents

List of figures

List of tables

Chapter 1.

Introduction

1.1. Enzymes

The term “enzyme” was first defined by Wilhelm Kilhe in 1877.[1] Enzymes are biocatalysts which can lower the activation energy and speed up chemical reactions. The discovery of Eduard Buchner, who won the Nobel Prize in Chemistry in 1907,[2] showed that fermentation process could take place without the presence of living cells. This suggested that there must exist substances responsible for connecting sugars. Eduard Buchner found and isolated the substance in yeast cell which can assist fermentation. This active substance was defined as enzyme.[2] The catalyst function of enzymes is of interest to many scientists who isolate them from living organisms in order to carry out fundamental or applied studies. James Batcheller Sumner found that the crystallized urease- which was to be protein – is also an enzyme.[3] In fact, most enzymes are proteins. However, some ribonucleic acids (RNA) also possess enzymatic activity. Enzymes act as catalysts in chemical reactions – they facilitate transformation of substrates into products (**Figure 1.1**). The high selectivity and high specificity are crucial for metabolic reactions taking place in all living systems. It is easier for human organism to absorb small molecules (*e.g.* glucose, maltose) as compared with large molecules (*e.g.* polysaccharides). However, during digestion, large molecules are hydrolyzed and broken down by enzyme into small molecules.

Figure 1.1 The general principle of enzyme-catalyzed reactions.

Enzymes are not only used by biological organisms, they are also utilized by industry in the production of food,[4] detergents,[5] paper,[6] textile material[7] and biofuel.[8] When using enzymes, many parameters of the reaction medium need to be adjusted, including: temperature, salinity, and acidity. Although it is not always straightforward to set the optimum conditions for the activity of enzymes, these potent catalysts are still very attractive for synthesis and

applications in analytical chemistry. Compared with traditional methods used by industry, enzyme-catalyzed reactions warrant low energy consumption, low production of toxic by companies.[9] Due to these advantages, enzymes and their applications are extensively studied by scientists.

1.1.1. Enzymatic reactions involved in adenosine triphosphate metabolism

Metabolic pathways leading to production of adenosine triphosohate (ATP) include glycolysis, citric acid cycle, and oxidative phosphorylation in aerobic metabolism or fermentation in anaerobic metabolism.[10, 11] The ATP molecule can be utilized as a substrate in various enzymatic reactions. For example, ATP can be hydrolyzed, and the released energy can be used in the processes of muscle contraction;[12] also, Moreover, adenosine residues resulting from enzymatic hydrolysis can be used to synthesize deoxyribonucleic acid (DNA) or RNA.[13, 14] ATP also plays a role in signal transduction processes. For instance, intracellular signaling – phosphate transfer –is catalyzed by kinase.[10] This enzyme facilitates removal of a phosphate group from substrate and transfers it to product. For example, pyruvate kinase is used to catalyze transformation of phosphoenol pyruvate (PEP) and adenosine diphosphate (ADP) for production of pyruvate and ATP. In glycolysis, the phosphate group is removed from PEP and transferred to ADP in one of the steps. Adenylate kinase is the enzyme that in particular to the adenosine nucleotides. Two molecules of ADP can be converted into one molecule of ATP and one molecule of AMP. The enzymatic reactions involved in the metabolic pathways related to ATP production are part of multi – enzyme systems such as the citric acid cycle.[15]

1.1.2. Enzymatic transesterification

The large amount of mechanical and electric equipment used by people all over the world contributes to the increased demand for energy. The main sources of energy include petroleum, coal and natural gas. By exploiting the common natural resources – which are very limited - the mankind contributes to a severe damage of the environment. The way to solve this problem is to find an alternative source of energy. Nowadays several alternative sources of energy are being exploited – for example, solar power, wind power, geothermal power and biodiesel. Due to the limitations of many alternative energy sources (in particular, solar and wind energy), biodiesel is considered as a promising energy source. Importantly, biodiesel

fuel can be produced on a large scale. The production of biodiesel often relies on the transesterification reaction.[16] The principle of this reaction is that one molecule of ester reacts with one molecule of alcohol and the acyl-containing moiety is transferred from the ester to produce another ester and a by-product. Esters and alcohols, such as triglycerides and methanol, are commonly used as the starting reagents, and they are converted to biodiesel (eq. 1.1, reproduced from ref.[6]).

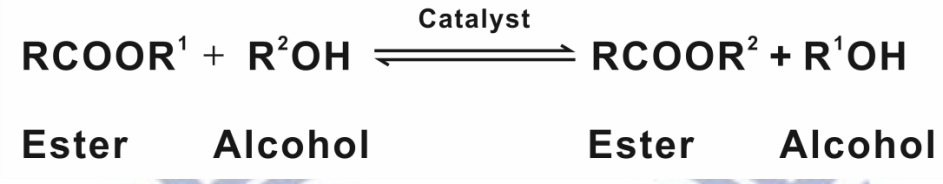

(eq. 1.1)

In order to speed up the transesterification reaction – a catalyst can be added to the reaction mixture. Acid, base or enzyme (lipase) can be used as catalysts. Using acid or base as catalyst is cheaper than using enzyme but this method has some drawbacks; for instance, the acid or base have to be removed after the reaction is finished. In this case, the treatment of post-reaction mixture has to be done – especially in the case of base. Compared to the other catalysts, the enzyme is a better choice it can be used to catalyze the reaction with high efficiency, either in aqueous or non-aqueous environment. In addition, it is much easier to remove the reaction by-products. Lipase enzymes are often used in transesterification reactions.[17] This process will be discussed further in Chapter 3.

1.2. Chromatography

The last three decades have brought significant developments in analytical methods involving chromatography,[18] electrochemistry,[19] optical spectroscopy and mass spectrometry.[20, 21] These powerful platforms allow one to perform qualitative and quantitative analysis of a variety of samples and compounds. For instance, separation power of chromatography is better than that of other separation techniques (*e.g.* extraction).[22] Chromatography was first used for the separation of plant pigments by Mikhail Tswett.[23] During the chromatographic process, the analyte mixture is pushed by mobile phase through the stationary phase – on the surface of a flat support, or inside a column. One can adjust the physicochemical properties of the mobile and stationary phases, so that every component of the mixture can be separated and recorded

by detector.

Chromatographic techniques are classified into numerous of categories. The three common chromatography techniques are as follows: (i) liquid chromatography, (ii) gas chromatography, and (iii) supercritical fluid chromatography.[24] Techniques can also be classified according to the type of mobile phase, column, and detection system. In one of the studies included in this project (Chapter 3), the analyzed molecules are volatile; therefore, gas chromatography was the first choice.

1.2.1. Parameter definitions and relations

In column chromatography, various factors affect separation. For example, diffusion coefficient of the analyte affects the contact of analyte with stationary phase.. Column efficiency can be calculated from the formula :

$$N = \frac{L}{H} \quad \text{(eq. 1.2)}$$

N: plate count

L: length of the column packing

H: plate height

According to the theory of chromatography,[25] the column efficiency increases with the increasing plate count and the decreasing plate height. The *van Deemter equation*[26] describes the dependencies between the plate height and system parameters:

$$H = A + \frac{B}{u} + Cu \quad \text{(eq. 1.3)}$$

or

$$H = \frac{B}{u} + C_S u + C_M u \quad \text{(eq. 1.4)}$$

A: eddy diffusion

B: longitudinal diffusion

C: mass-transfer term

C_S: mass-transfer term of stationary phase

C_M: mass-transfer term of mobile phase

u: linear velocity of mobile phase

Plate height (H) is one of the quantitative measures describing separation efficiency. The parameter A is related to the existence of multiple paths of molecules in a packed column. The parameter B describes formation of the analyte concentration gradient along the column. The parameter B influences separation in gas chromatography significantly because of the high diffusion rates in the gas phase. The parameter C relates to the mass transfer of the analyte between stationary phase and mobile phase.

Chromatographic resolution (R_s) describes the success or failure of separation. The resolution value tells us if two adjacent peaks are separated well or not. To calculate resolution, we focus on two neighboring peaks (A and B), and input their parameters to the following formula:

$$R_s = \frac{\Delta Z}{\frac{W_A}{2} + \frac{W_B}{2}} = \frac{2\Delta Z}{W_A + W_B} = \frac{2[(t_R)_B - (t_R)_A]}{W_A + W_B} \quad \text{(eq. 1.5)}$$

R_s: resolution

W: width of the peak

t_R: retention time

ΔZ: time interval between the peaks, $(t_R)_B - (t_R)_A$

1.2.2. Gas chromatography

Gas chromatography (GC) is a technique for separation of those analytes which can readily be transferred into gas phase. The separated compounds are driven by gaseous mobile phase, and they interact with the solid or liquid stationary phase. Since various compounds have different affinity to the stationary phase, their retention times are different. The interactions among the analyte, the mobile phase and the stationary phase are responsible for the separation. Archer John Porter Martin is the person credited for the development of the gas chromatography concept.[27] The main parts of a GC apparatus are (**Figure 1.2**):

(i) carrier gas system,

(ii) sample injection system,

(iii) column,

(iv) detector.

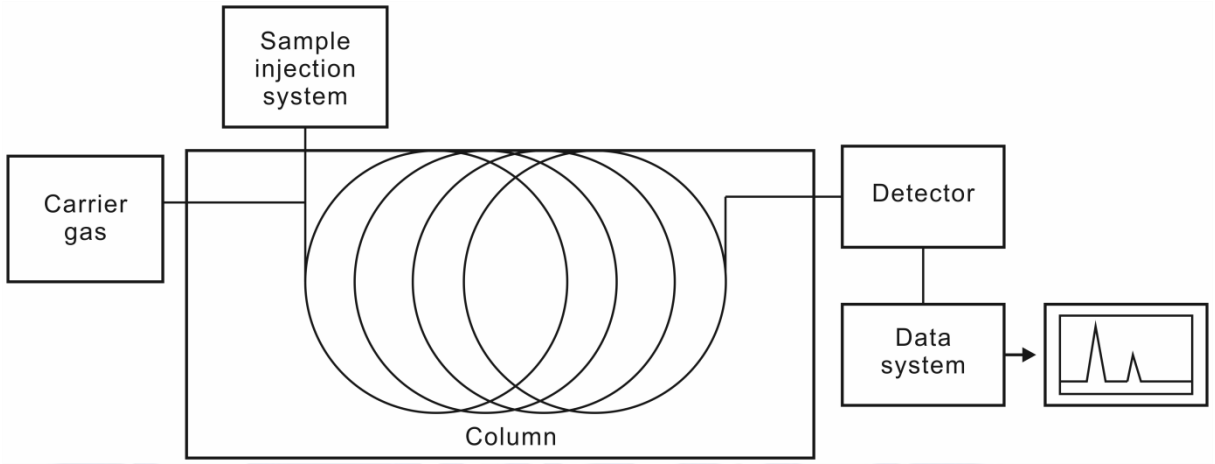

Figure 1.2 General scheme of gas chromatography apparatus.

1.2.3. Carrier gas system

The mobile phase in gas chromatography is controlled by the carrier gas system. Several gases are commonly used, including: helium, hydrogen, and nitrogen. Flow rate is measured by a flow meter, and maintained constant by pressure regulator. According to the *van Deemter equation* (eq. 3), type of carrier gas will affect the retention time and column efficiency. Helium, hydrogen and nitrogen are the most commonly used carrier gases in GC. The relation between the velocity of carrier gas and plate height is shown in **Figure 1.3**. Although nitrogen shows the lowest plate height among these three gases, the linear velocity – required to achieve the low plate height – is relatively low while slope of relation between plate height and velocity is high. Compared with helium and hydrogen, the hydrogen shows the low variances of change in wide range of linear velocity with plate height. However, the safety precautions of leakage of hydrogen should be taken into account. Due to these reasons, helium is chosen more often as a carrier gas as compared with nitrogen and hydrogen.

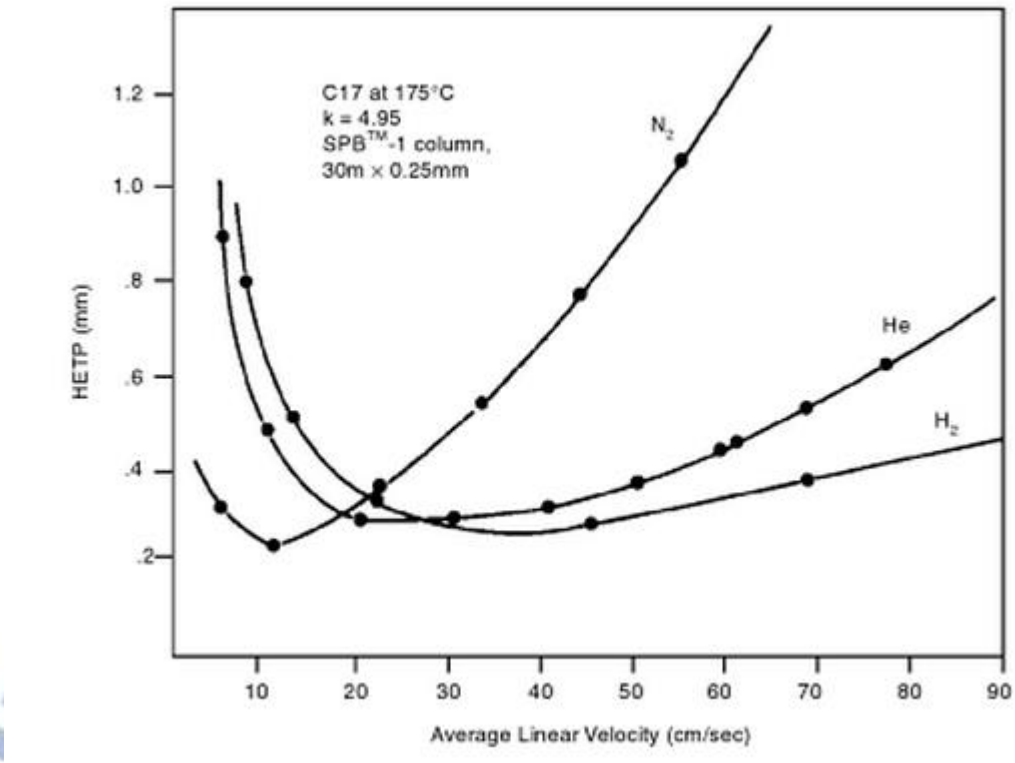

Figure 1.3 Relation between linear velocity of carrier gas and height equivalent to a theoretical plate (HETP). Reproduced from ref.[28]

1.2.3.1. Sample injection system

Both liquid and gas-phase samples can be introduced into GC column, either manually or automatically. In general, the temperature of the injection port assembly is set to be 50 °C higher than the boiling point of the least volatile component of the sample. In manual injection, or injection by autosampler, the needle of syringe is inserted into the injection port (**Figure 1.4**) via septum located at the GC inlet. The function of septum is to prevent the leakage of the carrier gas which would lead to mobile phase pressure instability. The sample is introduced to the liner cavity where vaporization occurs due to high temperature. The injection can be conducted in the split or splitless mode. The former is suitable for samples with high concentration of analytes while the latter is suitable for samples with low concentration. The column is connected to the bottom of the liner, so the vaporized sample can readily be guided by the flow of the carrier gas.

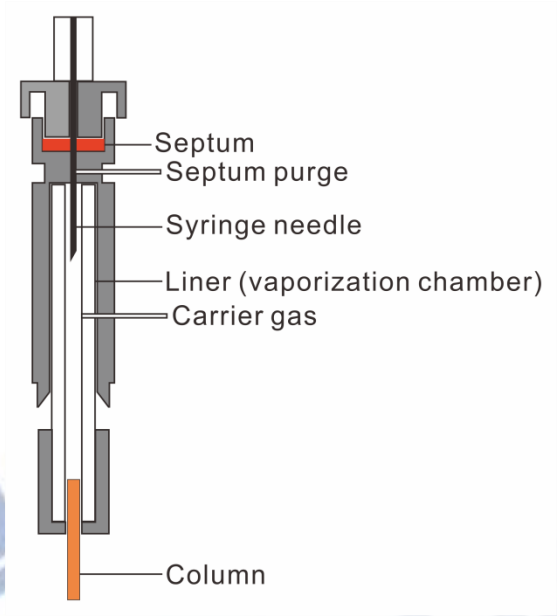

Figure 1.4 Injection port of gas chromatography apparatus. Sample is vaporized inside the chamber at high temperature after injection by syringe, and then it is carried by the mobile phase into column.

1.2.3.2. Column

Two types of columns are usually used in GC: (i) packed columns, and (ii) open-tubular (capillary) columns. Usually, the column efficiency of packed column is ~ 500-1000 N $m^{-1}$and for the open-tubular column is ~ 2000-4000 N m^{-1}(**Table 1.1**). Nowadays, open-tubular capillary columns are more popular than packed column due to the higher separation efficiency. Packed column is made of glass or metal tubing. Diatomaceous earth is the typical supporting material immobilized to the column. The stationary phase can be held by a supporting material with large surface area with small and uniform particle using diatomaceous earth. The separation performance of packed columns heavily depends on the particle size of the supporting material.

There are three basic types of open tubular (capillary) columns which differ by the types of stationary phase coated onto the inner wall: wall-coated open tubular (WCOT) columns and support-coated open tubular (SCOT) columns.[28] Fused-silica wall-coated open tubular columns (FSWC) are the third type of open-tubular column and widely used recently. FSWCs feature: small inner diameter (0.1 – 0.3 mm); length from 10 to 100 m; and relatively low back pressure. The efficiency of FSWCs is much higher than that of other types of columns mentioned above (WCOT, SCOT, packed columns); **Table 1.1**.

Table 1.1 Comparison of typical gas chromatography columns. Modified from ref.[71]

	Type of column			
	FSWC	**WCOT**	**SCOT**	**Packed**
Length, m	10-100	10-100	10-100	1-6
Inner diameter, mm	0.1-0.3	0.25-0.75	0.5	2-4
Efficiency, plates / m	2000-4000	1000-4000	600-1200	500-1000
Sample size, ng	10-75	10-1000	10-1000	10-106
Relative pressure	Low	Low	Low	High
Relative speed	Fast	Fast	Fast	Slow
Flexibility	Yes	No	No	No
Chemical inertness	Best	Good	Fair	Poor

Stationary phase plays an important role in GC separation. There are several requirements for the choice of stationary phase. The material of stationary phase should have the following properties: (i) low volatility, (ii) thermal stability, and (iii) chemical inertness. The materials frequently used as stationary phase are polydimethylsiloxane (PDMS) and phenylpolydimethylsiloxane.[28] By changing the functional groups of stationary phase, the polarity can be changed, and such columns can be applied in the analyses of a variety of compounds.[29]

1.2.3.3. Detection systems

There are a number of detectors commonly used in GC. Ideally, the detector should exhibit the following characteristics: high sensitivity, reproducibility, stability, operation in a wide temperature range, short response time. Several common detectors used in GC are listed in **Table 1. 2**.

Notably, flame ionization detector (FID) is widely used detector in GC. In FID, the separated compounds are introduced into an air/hydrogen flame. As a result, ions and electrons are produced. The electric current (~ 10^{-12} A) in the electrode circuit is measured and used as the output signal of the detector. Other detectors – thermal conductivity detector , electron-capture detector , and mass spectrometric detector – are also popular. Mass spectrometric detector is great for identification of compounds in a mixture and further capable of doing quantitative analysis. Due to the mass spectrometry detector was chosen as the detector in this study, the detail information will be discussed later in this chapter.

Table 1.2 Typical detectors for gas chromatography. Modified from ref.[71]

Type	Applicable sample	Typical detection limit
Flame ionization	Hydrocarbons	1 pg/s
Thermal conductivity	Universal detector	500 pg/mL
Electron capture	Halogenated compounds	5 fg/s
Mass spectrometer (MS)	Tunable for any species	0.25 - 100 pg
Thermionic	Nitrogen and phosphorous compounds	0.1 pg/s (P), 1 pg/s (N)
Electrolytic conductivity	Compounds containing halogens, sulfur, or nitrogen	0.5 pg/s (Cl), 2 pg/s (S), 4pg/s (N)
Photoionization	Compounds ionized by ultraviolet radiation	2 pg/s (C)
Fourier transfer Infrared	Organic compounds	0.2 - 40 ng

1.2.3.4. Applications of gas chromatography

GC is a powerful platform for the analysis of volatile and thermally stable samples. Qualitative and quantitative analyses are conducted in many areas, including environmental and food analysis as well as quality control of pharmaceuticals and other chemical products.[30-32] Moreover, in the field of forensic,[33] GC is used to trace the residues from the scene of a fire, and then to identify the volatile compound which could be the cause of the fire.[34] In addition, GC is used by security officers for detection of explosive substances and prevention of the acts of crime.[35]

1.2.3.5. Qualitative analysis

In many cases, the analyzed samples are mixtures of unknown compounds which need to be identified. GC has a great potential for identification of unknown molecules. The retention times of every peak are linked to the physicochemical properties of the separated molecules which interact with the stationary phase. There are established criteria for identifying certain compounds. For example, the retention index (*I*) was defined by Eugen Kovats in 1958.[36] This index is related to the number of carbon atoms of normal alkanes. The numbers of carbon atoms is the molecule of unknown compounds can be estimated based on calculated the retention indices. In general, it takes a considerable amount of time to separate a mixture of compounds in a GC column kept at a constant temperature. In the case of challenging separations, and in order to speed up analyses, one often implements temperature programming. In this process, the oven temperature is increased stepwise or gradually, so that

more volatile compounds can be resolved at a lower temperature while less volatile compounds are not retained inside the column for too long. Although the chromatographic resolution and the analysis time can be improved this way, the interpretation of the resulting retention times is less straightforward as compared with the data obtained using constant column temperature setting. In order to minimize the limitations of GC in the identification of unknown molecules, it is beneficial to hyphenate it with mass spectrometric or optical spectroscopic detectors (see also section **1.2.3.3.**), what can provide orthogonal data required for identification. The results of analyses conducted on such hyphenated systems are information-rich, and the data obtained using the two analytical platforms (*e.g.* retention times from GC and *m/z* values from MS) complement each other.

1.2.3.6. Quantitative analysis

In many applications, it is important to determine the exact amount of analyte present in the sample. Usually, the peak height or peak area in the gas chromatogram one used to make calibration plots – the correlation between signal response and analyte concentration. From such plots, quantities or concentrations of the analytes can be determined. However, a number of factors such as sample loss with high volatility or uncertainties error of injection may affect quantification in GC. In order to eliminate possible errors, an internal standard should be added to the sample. Usually, it is suggested that the chemical and physical properties of the internal standard should be similar to those of the target compound. However, the compound used as the internal standard should not be present in the original sample. In the best case, during the processes of sample preparation and analysis, the internal standard should be handled in the same way as the target analyte. During data processing, the signal of the target analyte is divided by the signal of the internal standard. Many sample preparation and metering-related errors are removed this way. To achieve quantitative analysis, a calibration plot should be constructed based on the signals from target compound and internal standard obtained in the same runs.[37]

1.3. Mass spectrometry

Mass spectrometry (MS) is used in a variety of analyses which require high sensitivity. It enables both qualitative and quantitative analysis. There are several major parts of every mass spectrometer, most importantly: (i) ion source, (ii) mass analyzer, and (iii) detector (**Figure**

1.5). First, the sample is ionized and transferred into the gas phase. Second, ions are separated in the presence of electric field or magnetic field, and finally the separated ions are driven to the detector. The signals of the detected ions are recorded by a computer system.

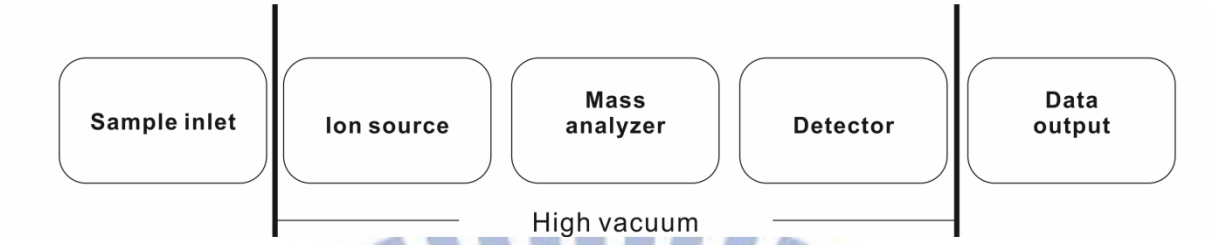

Figure 1.5 General scheme of mass spectrometry system.

1.3.1. Ion source

1.3.1.1. Electron ionization

The work described in this thesis was done using two mass spectrometers, one of which was coupled with the electron ionization (EI) source (**Figure 1.6**). Substances separated on GC column are eluted, and then transferred to the EI. Next, the newly formed ions are guided in the presence of applied electric field and separated in the mass analyzer.. EI sources in GC-MS systems commonly use a 70 eV electron beam. The electrons are produced by a filament wire or coil. The gas-phase molecules are ionized and fragmented due to collisions with electrons.

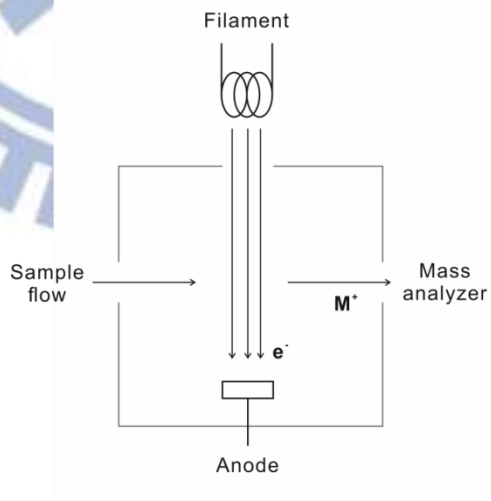

Figure 1.6 The principle of electron ionization source.

1.3.1.2. Electrospray ionization

Electrospray ionization (ESI) is one of the most powerful ion sources. It was developed by John Bennett Fenn *et al*.[38] The invention received the Nobel Prize in chemistry in 2002..[39] In the first ESI setup, large biomolecules were successfully ionized, and analyzed on a quadrupole mass analyzer. Importantly, intact ions could be observed and multiply charged fragments could be used to estimate the molecular weights of the large species. Compounds with molecular weight up to 130 kDa could be detected. In recent year, some results show that ESI-MS can detect the molecular weight on the level of millions of Da.[40] This is in stark contrast to the older ionization methods such as EI.

In ESI, the sample solution is delivered hydrodynamically via a stainless steel needle. A high potential of a few thousand volts is applied to the needle positioned at the inlet of mass spectrometer. Application of a positive potential to the needle will likely produce positively charged ions. In this case, the positive ions are repelled by the voltage applied to the needle while negative ions are attracted toward the inner wall of the needle. When positive charge accumulated at the tip of needle, the sample solution acquires conical shape. This phenomenon is referred to as "Taylor cone". Charged droplets are formed. Once repulsive force exceeds the surface tension, "Coulomb explosion" occurs at the tip of the Taylor cone. The droplets and the newly formed ions are guided toward the inlet of the mass analyzer. The nebulization gas, applied coaxially to the metal needle, can further assist desolvation of the charged droplets, and transfer the ions into the gas phase. Finally, the ions are migrated to the mass analyzer and then to the detector (**Figure 1.7**).[41-43]

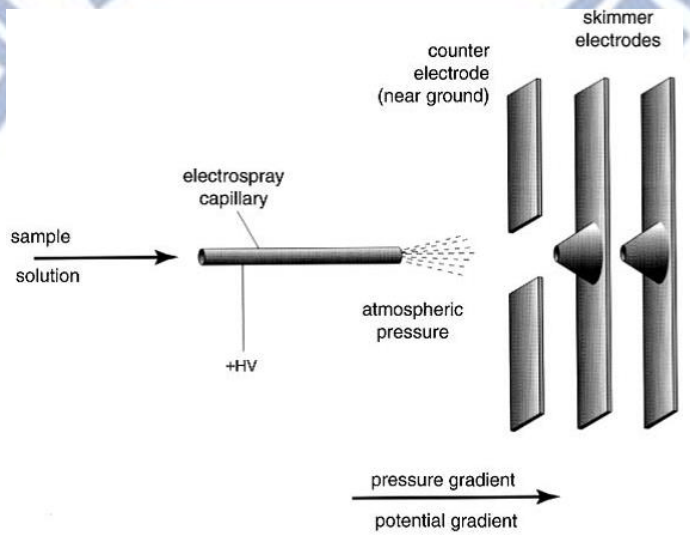

Figure 1.7 Scheme of the electrospray ionization system. Modified from ref.[41]

1.3.1.3. Venturi easy ambient sonic-spray ionization

Atmospheric pressure ionization allows one to create ions from the sample directly in the atmospheric pressure conditions instead of high vacuum conditions, without the sample pretreatment and separation. Apart from ESI, some new ionization methods are developed. For example, desorption electrospray ionization invented by Takáts *et al.*[44] is one of the representative atmospheric pressure ion sources in past few years, the sample can be ionized in an atmospheric interface with high speed aqueous spray induced by high voltage and optimized angle between aqueous spray and sample. This technique has various advantages: for example, no sample pretreatment, direct analysis of the sample and continuous detection. Other techniques of atmospheric pressure ionization methods were also presented; for instance, direct analysis in real time,[45] electrospray-assisted laser desorption/ionization[46].

In order to monitor enzymatic reactions using mass spectrometry, a compatible interface between the reaction chamber and mass spectrometer to be constructed. After taking into account all compatibility issues, Venturi easy ambient sonic-spray ionization (V-EASI) was believed to be the best choice for the proposed research.[47] The V-EASI takes advantage of the Venturi effect.[48] Venturi effect occurs in a fluidic system when reduction of pressure happens due to the passage of fluid through a constricted section. In our setup, the nitrogen gas flow is applied to the T-junction, and flows out from a narrow capillary (**Figure 1.8**). A negative pressure is created, and it induces flow of sample in the probe capillary. The sample solution is sprayed out, and liquid droplets are produced. The high temperature and dry gas assist desolvation of resulting droplets, and transfer of the newly formed ions into the gas phase. Then ions are guided subsequently to mass analyzer in the presence of the gas flow at the Venturi pump assembly.

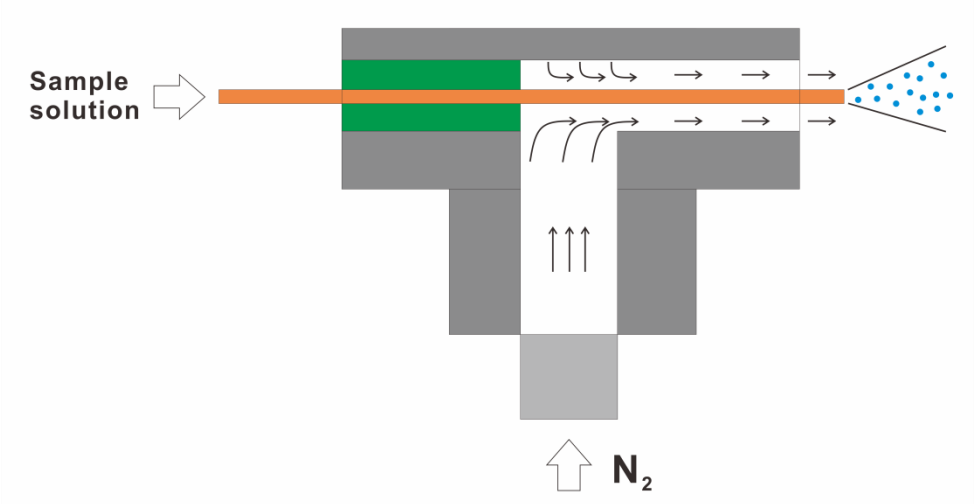

Figure 1.8 Schematic of a modified Venturi easy-ambient sonic spray ionization source used in this study. Compared to the original version in ref.[45]

1.3.2. Mass analyzer

Numerous types of analyzers are used in mass spectrometry. For example, quadrupole mass analyzers are commonly coupled with GC systems and EI sources while ion traps often accompany the systems equipped with ESI sources. The following sections (**1.3.2.1** and **1.3.2.2**) briefly outline quadrupole and ion trap mass analyzers – used in this work (Chapters 2 and 3).

1.3.2.1. Quadrupole

The quadrupole mass analyzer comprises two pairs of parallel metal electrodes (**Figure 1.9**). These electrodes are connected to the sources of direct current (DC) and alternating current (AC). When the charged species enter the analyzer, they are separated due to interaction with the electric field. The DC and AC voltages can be adjusted in a way that only the ions with specific *m/z* values attain stable trajectories passing along the whole length of the electrodes. The other ions collide with the electrodes or other surfaces in the analyzer cavity. The ions-passing through the quadrupole zone – eventually reach the detector.[22]

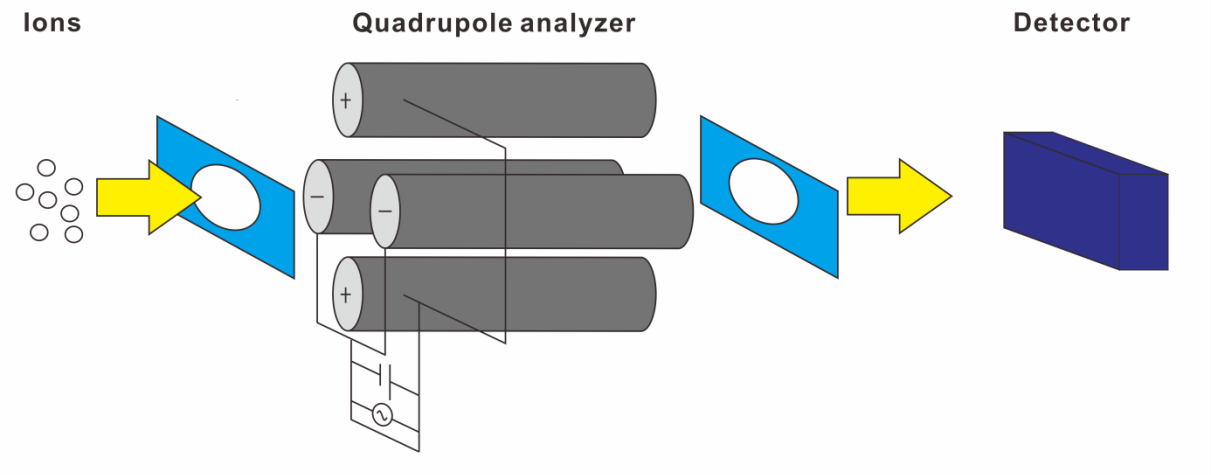

Figure 1.9 Schematic representation of the quadrupole mass analyzer.

1.3.2.2. Ion trap

The ion trap instrument was invented by Wolfgang Paul and Helmut Steinwedel.[49] It comprises two end cap electrodes and one ring electrode, located between the end cap electrodes (**Figure 1.10**). A DC voltage is applied to the end cap electrodes. An AC voltage is applied to the ring electrode in order to facilitate trapping ions inside the cavity between the electrodes. The motion of ions, controlled by the AC electric field, is described by the Mathieu equation.[50] The ions are subsequently ejected from the trapping region toward the detector, giving rise to an electric signal which can be recorded by the data acquisition system. One of the prominent advantages of ion trap is its ability to perform tandem mass spectrometry (MS/MS) – useful in the identification of unknown compounds.[51]

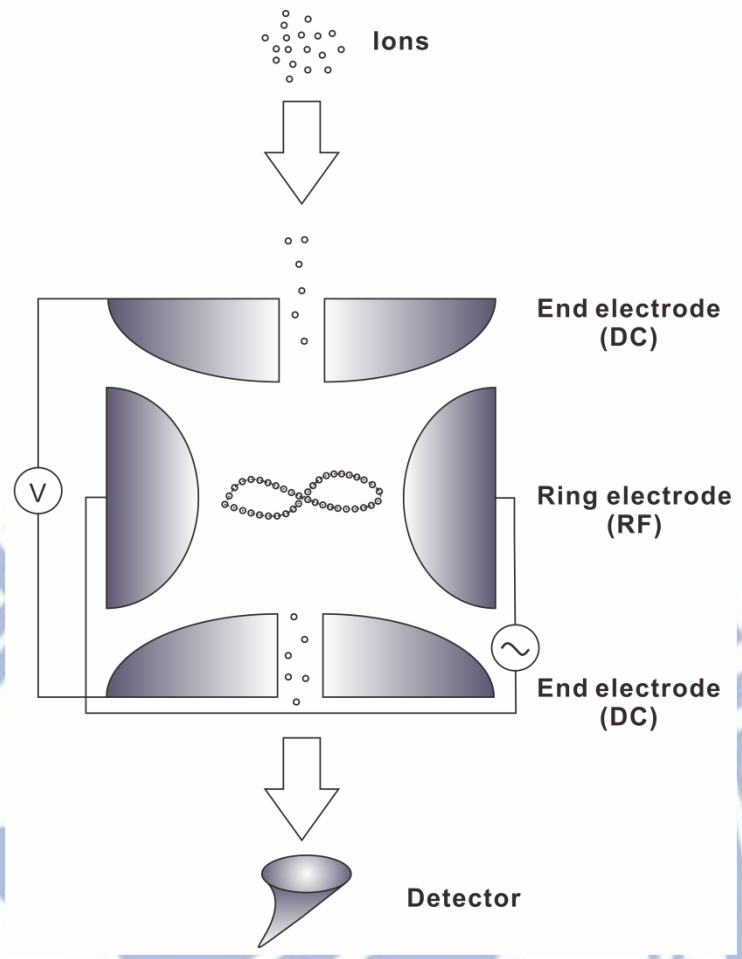

Figure 1.10 Schematic representation of ion trap mass analyzer.

1.4. Goals of the study

In this study, we focused on detecting the biocatalytic ability of model enzymatic reactions. In particular, we highlight the possibility to conduct monitoring dynamic system by mass spectrometry. We aimed to develop mass spectrometric methods for the monitoring of enzymatic processes. The goal of the study described in Chapter 2 was to develop a method to monitor a bioautocatalytic reaction using mass spectrometry at atmospheric pressure by using a simple platform with reaction chamber and atmospheric pressure ionization method. The behavior of the bienzymatic reaction needed to be observed in real time analysis. The goal of the study described in Chapter 3 was to develop an interface for sampling dynamic systems (*e.g.* an enzymatic reaction), and transfer the sample aliquots to a GC-MS apparatus for instantaneous analysis. The model reaction was catalyzed by the enzyme immobilized onto the porous microbeads. Moreover, we intended to provide a catalytic ability assay targeting single beads of the immobilized enzyme.

Chapter 2.

Spatiotemporal effects of a bioautocatalytic chemical wave revealed by time-resolved mass spectrometry

2.1. Introduction

In nature, diffusion (movement of molecule from the zone with high concentration to the zone with low concentration) and convection (bulk / collective movement of substance or energy in a fluid) are responsible for translocation of chemical molecules over micro- and macro-scopic distances. Diffusion uses internal energy to equalize concentrations of substances in the surrounding space, while convection is responsible for collective movement of molecules in a field gradient. Both processes underlie interactions occurring between chemical molecules. They ascertain mixing of substances in chemical reactors, and enable communication between cells in tissues.[52] In various components of biomolecular machinery, a faster transport (or chemical signal transduction) is required than that provided by diffusion and convection. Nature has invented efficient ways of transmitting molecules and chemical signals, which are faster than those enabled by diffusion and convection. For example, proteins are actively moved within biological cells along the fibres of cytoskeleton, so that they can be delivered quickly to specific locations.[53] In artificial systems, diverse pumping methods are used: for example, hydrodynamic[54] or electroosmotic[55] flow can be exerted on a fluid by using a syringe pump or an electrical power supply, respectively. It is also known that reaction-diffusion systems lead to formation of moving fronts.[56, 57] They are driven by the difference between the chemical potentials of the reactants and the products. Other studies also revealed that even common chemical reactions – such as acid-base neutralization – can produce hydrodynamic instabilities,[58] inducing macroscopic movements of chemical molecules. Due to the growing interest in bioengineering, it would be desirable to possess a method of transmitting chemical signals over macroscopic distances – in a controlled manner – without the reliance on mechanical or electrical devices, which would be compatible with biochemical systems. A suitable candidate for such a method would be an enzymatic

autocatalytic process.

Here we describe a semi-artificial chemical process incorporating a bienzymatic reaction, which is capable of generating chemical waves that propagate over macroscopic distances in a liquid medium at room temperature – faster than diffusion and convection. It is based on a bienzymatic reaction system[59, 60] using adenosine diphosphate (ADP) and adenosine triphosphate (ATP) as the carriers of chemical signal:

$$\mathbf{ATP} + \mathrm{AMP} \xrightarrow{\text{adenylate kinase}} 2\mathbf{ADP} \qquad \text{(eq. 2.1)}$$

$$\mathbf{ADP} + \mathrm{PEP} \xrightarrow{\text{pyruvate kinase}} \mathbf{ATP} + \mathrm{PR} \qquad \text{(eq. 2.2)}$$

According to the above scheme, ATP is the substrate in reaction (1) and the product of reaction (2). Conversely, ADP is the substrate of reaction (2) and the product of reaction (1). The key feature of this autocatalytic system is that, in reaction (1), 2 molecules of ADP are synthesized out of one molecule ATP. This subsequently doubles the number of ATP molecules produced in reaction (2). Hence, the number of cycling ADP and ATP molecules will double in each sequence, while the co-substrates (adenosine monophosphate (AMP) and phosphoenolpyruvate (PEP)) are consumed, and a by-product (pyruvate, PR) is formed. Since none of the products of reactions (1) and (2) absorb light in the visible part of electromagnetic spectrum, it is not easy to follow spatiotemporal characteristics of the process. Therefore, in order to demonstrate the concept outlined above, we implemented a time-resolved mass spectrometry[61] approach, which enabled monitoring of the non-chromogenic ionizable reactants in real time, and with an adequate temporal resolution. In fact, time-resolved mass spectrometry offers important advantages in such experiments because: fast-changing reactants of an autocatalytic process can be monitored with minimum cross-interferences; with high selectivity, sensitivity, and speed.

2.2. Experimental section

2.2.1. Materials

Ammonium acetate, adenosine 5′-monophosphate monohydrate (AMP), adenosine 5′-triphosphate disodium salt hydrate (ATP), adenosine-$^{13}C_{10}$ 5′-triphosphate sodium salt

solution ($^{13}C_{10}$-ATP), ethylenediaminetetraacetic acid (EDTA) tetrasodium salt dihydrate, potassium chloride, and magnesium sulfate were Sigma-Aldrich (St Louis, USA). Phosphoenolpyruvic acid monopotassium salt was from Alfa Aesar (Ward Hill, USA). The two enzymes – adenylate kinase (myokinase from chicken muscle, catalogue No. M5520, essentially salt-free, lyophilized powder, 1,500-3,000 units mg^{-1} protein) and pyruvate kinase (from rabbit muscle, catalogue No. P9136, type III, lyophilized powder, 350-600 units mg^{-1} protein) – were from Sigma-Aldrich. On arrival, the enzymes were dissolved in 1 mL 10^{-2} M ammonium acetate to reach the specific activities of 1,000 U mL^{-1}. The fused silica capillary with the ID 150 μm (OD 375 μm) – used in the Venturi pump assembly – was obtained from GL Science (Tokyo, Japan).

2.2.2. Apparatus and procedure

In the beginning of the experiment, the drift cell (standard NMR tube with perforated bottom) was filled with a solution of enzymes, the main substrates (except ATP), cofactors, and buffer components (**Figure 2.1A**). The composition of the reaction medium was: 10 mM ammonium acetate, 0.1 mM EDTA, 0.1 mM potassium chloride, 0.1 mM magnesium sulphate, 0.1 mM AMP, 0.1 mM PEP, 10 U pyruvate kinase, and 10 U adenylate kinase. In the experiment involving demonstration of accelerated transduction, adenylate kinase was added to the reaction mixture right before loading the drift cell. In the experiment involving demonstration of passive transduction, adenylate kinase was not included in the medium, so the cycling reaction (eq. 2.1 and 2.2) could not proceed. Special precautions were taken to prevent introduction of air bubbles. The drift cell was placed horizontally in a holder attached to the *xyz*-stage placed in from of the mass spectrometer. Fused silica capillary (ID 150 μm, OD 375 μm; GL Science, Tokyo, Japan) attached to Venturi pump (1/8-inch stainless steel tee; Swagelok, Supelco; Solon, OH, USA) was inserted into the drift cell, so that the distance between the inlet of the drift cell, and the inlet of the fused silica capillary, was ~ 4 cm. While the outlet of the drift cell was open, the inlet was hydraulically connected to a 100 μL glass syringe filled with the ATP solution (also containing the buffer components as for the enzymatic reaction). The reaction solution was held inside the open tube due to cohesive and adhesive forces. Nitrogen gas was supplied to the Venturi pump (pressure: ~ 207 kPa) in order to induce suction of the liquid sample, nebulization, and ionization of the analytes in front of the orifice of a mass spectrometer. The flow rate of the sample solution in the fused silica capillary was ~ 840 μL h^{-1}. Such low flow rate does not produce significant advective

movement of the solution inside the drift cell. Much of the liquid aspirated by the Venturi pump originates from the section of drift cell downstream from the inlet of the fused silica capillary (closer to the open end of the drift cell), and a small fraction of the aspirated liquid comes from the end section of the 4-cm long drift region. After setting up the drift cell, data acquisition was started, and the syringe pump was set to inject 30 μL of the ATP solution with the flow rate of 20 μL min^{-1}. Following the injection of the trigger ATP – which took 90 s – the syringe pump was on stand-by.

In order to monitor the propagation of chemical waves (either due to classical phenomena or accelerated transduction of chemical signals) we used an ion trap mass spectrometer (amaZon speed; Bruker Daltonics, Bremen, Germany) operated in the negative-ion mode. The voltage applied to the ion transfer capillary was 2500 V, and the end-plate offset was set to 500 V. The flow rate of the dry gas was set to 6.5 L min^{-1}. The mass range was set to 15-700 u e^{-1}. The data were collected with TrapControl software (ver. 7.1; Bruker Daltonics), exported to ASCII files, and further treated in Excel (2010; Microsoft, Redmond, WA, USA).

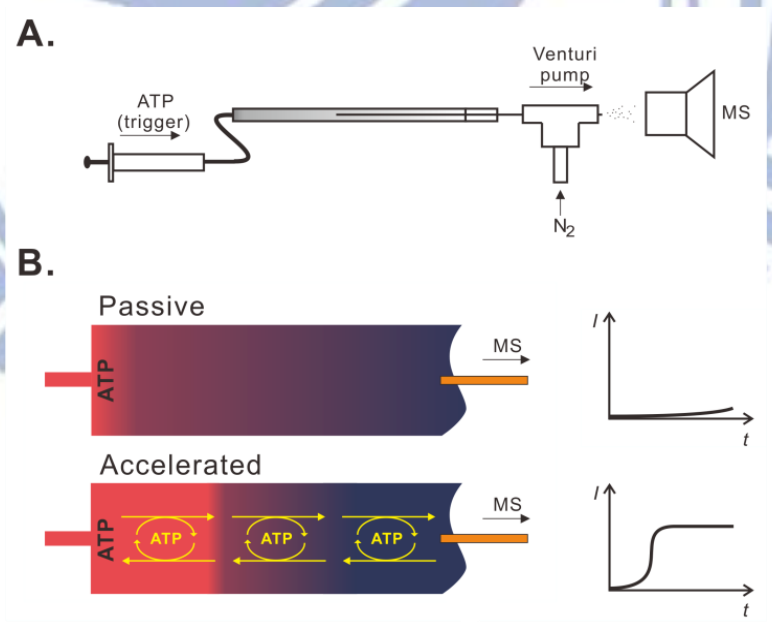

Figure 2.1 Investigation of a chemical wave due to "passive" transduction and bienzymatic amplification system (eq. 2.1 and 2.2). (A) Experimental setup incorporating a horizontal drift cell and mass spectrometer. (B) Schematic representation of chemical wave propagation in the drift cell due to the passive and the enzyme-accelerated transduction.

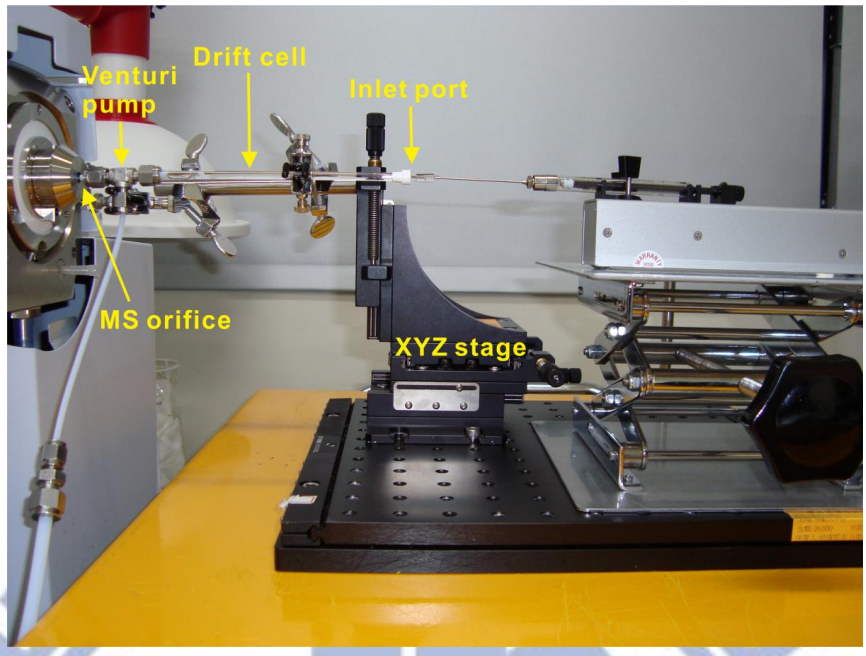

Figure 2.2 Experimental setup used for testing the speed of propagation of classical mass transport (due to diffusion and convection), and the proposed reaction-aided chemical wave.

2.3. Results and discussion

2.3.1. Verification of wave propagation

In order to verify the possibility of transmitting chemical signals (ADP/ATP) over a macroscopic distance, we used a simple experimental setup (**Figure. 2.1A**) comprising a horizontal tube with a high aspect ratio (drift cell) with inlet and outlet ports. The drift cell was filled with the mixture of all the reactants and enzymes required for the bienzymatic process (reactions, eq. 2.1 and 2.2) except for ADP and ATP. The outlet port of the drift cell was connected to the Venturi pump11 providing a constant but relatively low suction force. The reaction solution was constantly probed, and transferred to the ionization zone of the ion trap mass spectrometer. The inlet port of the drift cell was connected to a syringe filled with ATP solution. A small aliquot of ATP solution (~ 30 μL) was dispensed in order to trigger the chemical wave. The chemical wave propagated over the distance of 4 cm – measured from the inlet port of the drift cell to the inlet of the capillary incorporated into the Venturi pump assembly (**Figures 2.1A** and **2.2**). Importantly, the volume of this 4-cm long section corresponds to 600 μL. Thus, the injection of 30 μL ATP solution (5% of the drift volume) has negligible contribution to advective motion inside the drift cell.

Figure 2.1B illustrates two alternate schemes of the propagation of chemical wave in the

drift cell, based on passive (top) and accelerated (bottom) transduction. We hypothesized that chemical wave carried by the enzymatic reactions in (1) and (2) will transmit the ATP signal towards the outlet port of the drift cell faster than passive transduction due to diffusion and convection along with the advective motion induced by the Venturi pump. An initial hypothesis was that the reactions (1) and (2) can rapidly elevate local concentration of ADP/ATP as soon as a small amount of these species is brought to an ADP/ATP-free region of the reaction medium. Therefore, convection and diffusion would only be needed to propel the chemical wave in microscale, while the autocatalytic reaction system would accelerate its propagation along the drift volume. This hypothesis was verified using time-resolved mass spectrometry as a tool of chemical analysis in real time. To simplify evaluation of the mass spectrometric data, the signal intensities (*I*, integral of signal intensities across a short section of mass spectrum near the peak centroid, $\pm$ 0.5 u e^{-1}) corresponding to the signals of AMP, ADP, and ATP (*cf*. **Figure 2.3**) were computed according to the formula:

$$\text{Rel. yield} = \frac{I_{\text{ADP}} + I_{\text{ATP}}}{I_{\text{AMP}} + I_{\text{ADP}} + I_{\text{ATP}}} \quad , \qquad \text{(eq. 2.3)}$$

smoothed, and plotted against time (**Figure 2.4**). The reaction was run with an optimized and characterized composition of the reactant mixture (cf. **Figure 2.3**). In **Figure 2.4**, one can clearly see the difference between the two cases corresponding to the passive and the accelerated transduction, respectively. The upper graph in **Figure 2.4** shows the result of an experiment in which adenylate kinase was not included in the reaction cocktail. Therefore, the cycling bienzymatic reaction did not occur. The bottom graph in **Figure 2.4** shows the result of an experiment in which both enzymes were present in the reaction cocktail. In the former case, the propagation of ATP was mainly due to convection and diffusion, superimposed with the advective motion arising in the drift cell (passive transduction). In the latter case, amplification of ATP could take place. Therefore, the fast appearance of ATP is attributed to the bienzymatic reaction which increases local concentration of ATP ion of ATP latter case, amplification of available to trigger the cycling process (accelerated transduction). This result confirms the hypothesis illustrated in **Figure 2.1B** showing the feasibility of using the bienzymatic system in eq. 2.1 and 2.2 to propagate a chemical wave with a speed higher than it would result from the classical mass transport (**Figure 2.1A**).

The ratios of the relative yield in the end of the run (3200-3600 s) to the relative yield in the beginning of the run (600-1000 s; *cf.* yellow dashed frames in **Figure 2.4**) were 4.5 and

21.4, in the case of passive and accelerated transduction, respectively (values calculated without prior normalization of datasets). This shows a relative gain of the chemical signal corresponding to an elevated concentration of ADP and ATP. These differences are also visible in the unprocessed extracted ion currents (**Figure 2.6**). While the result in **Figure 2.4** (top, passive transduction) exhibits an elevation of trace at the end of the run, the exact timing of the arrival of chemical wave in this experiment was not perfectly reproducible. This is because the liquid inside drift cell is not perfectly quiescent. The temperature gradient in front of the mass spectrometer, and the hydrodynamic flow exerted by the Venturi pump used for ionization, induce advective movements inside the tube. Formation of local eddies – near the inlet of Venturi pump capillary – can lead to chaotic mixing inside the drift cell and instabilities of the MS signal. Instabilities of experimental conditions (*e.g.* occurrence of temperature gradient in front of MS, decay of enzymatic activity) may be responsible for unsatisfactory reproducibility of the obtained results. Therefore, comparison of the results can only be valid if the two experiments (involving passive and accelerated transduction) are carried out in a series – using the same setup and conditions. We tried to assure this as much as possible but also sought another dependable method to investigate the enzyme-accelerated chemical waves.

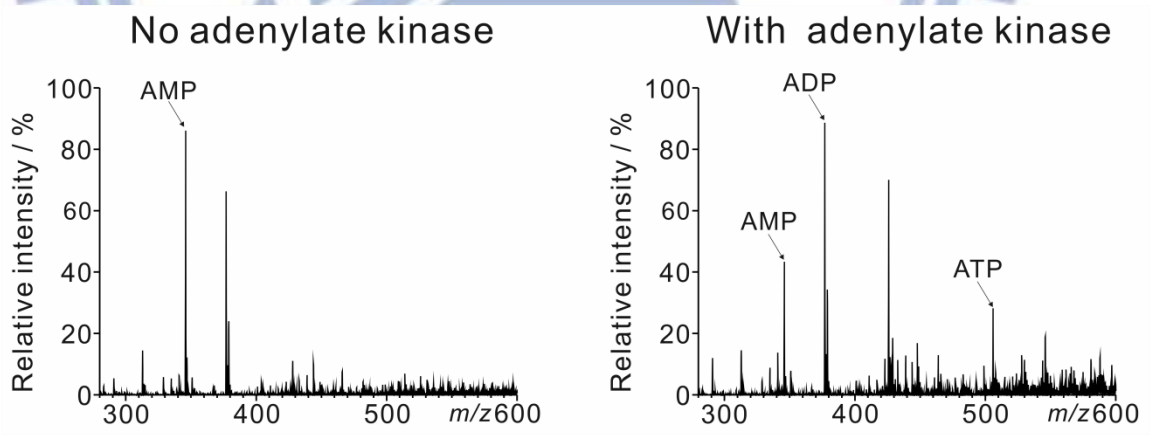

Figure 2.3 Optimization of the bienzymatic reaction system (eq. 2.1 and 2.2). Representative mass spectra obtained after incubation of reactants with pyruvate kinase (left), or pyruvate kinase and adenylate kinase (right; incubation time: 60 min).

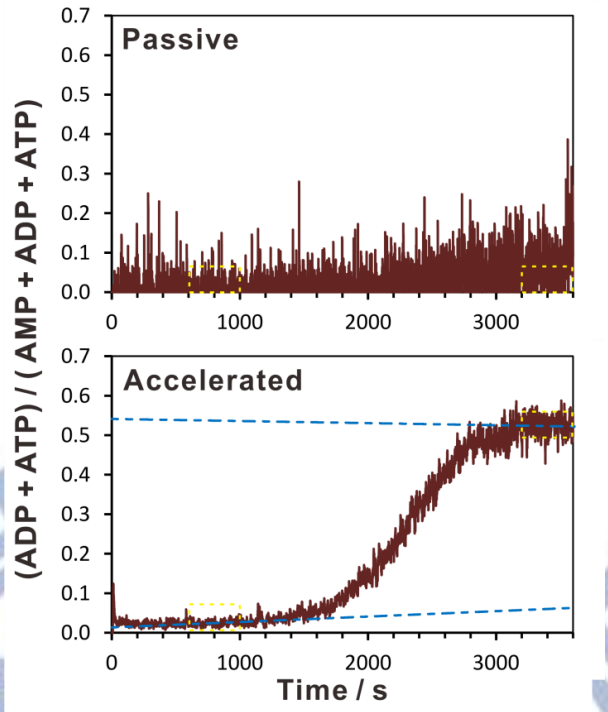

Figure 2.4 Propagation of a bioautocatalytic chemical wave in a horizontal drift cell, recorded online by time-resolved mass spectrometry: passive (top) *vs.* accelerated transduction (using the bienzymatic reaction system; bottom). Concentration of the trigger ATP: 5×10^{-3} M. **Figure 2.6** presents unprocessed extracted ion currents from this experiment. Exponential smoothing with a time constant of 4.1 s has been applied. Yellow dashed frames indicate the time ranges for which average relative intensities were calculated (see the narrative text for explanation). Blue dashed lines are linear functions fitted to the datasets highlighted with yellow dashed frames to facilitate visual assessment.

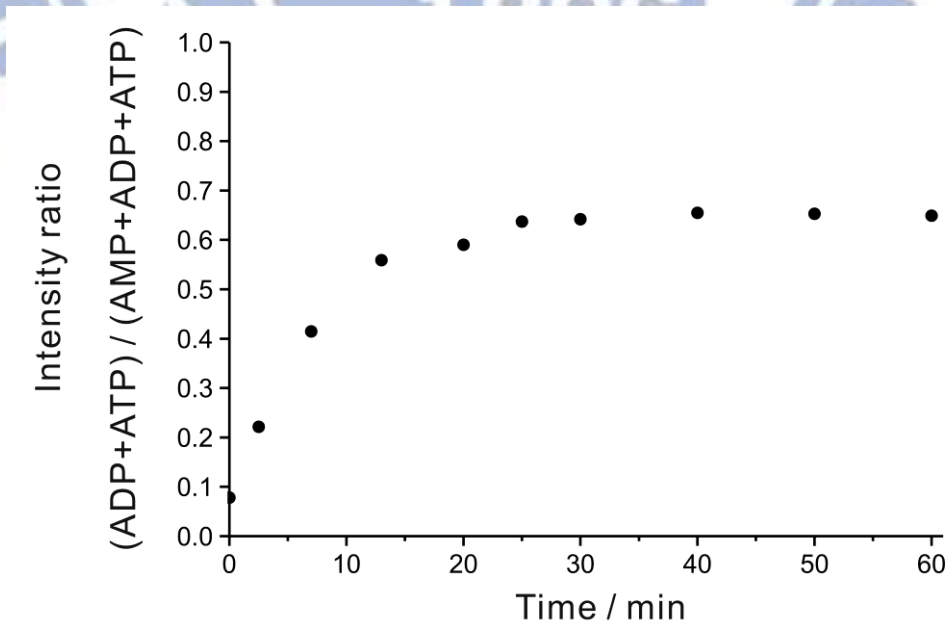

Figure 2.5 Time progress of the *in-vitro* synthesis of ADP/ATP recorded by mass spectrometry during optimization.

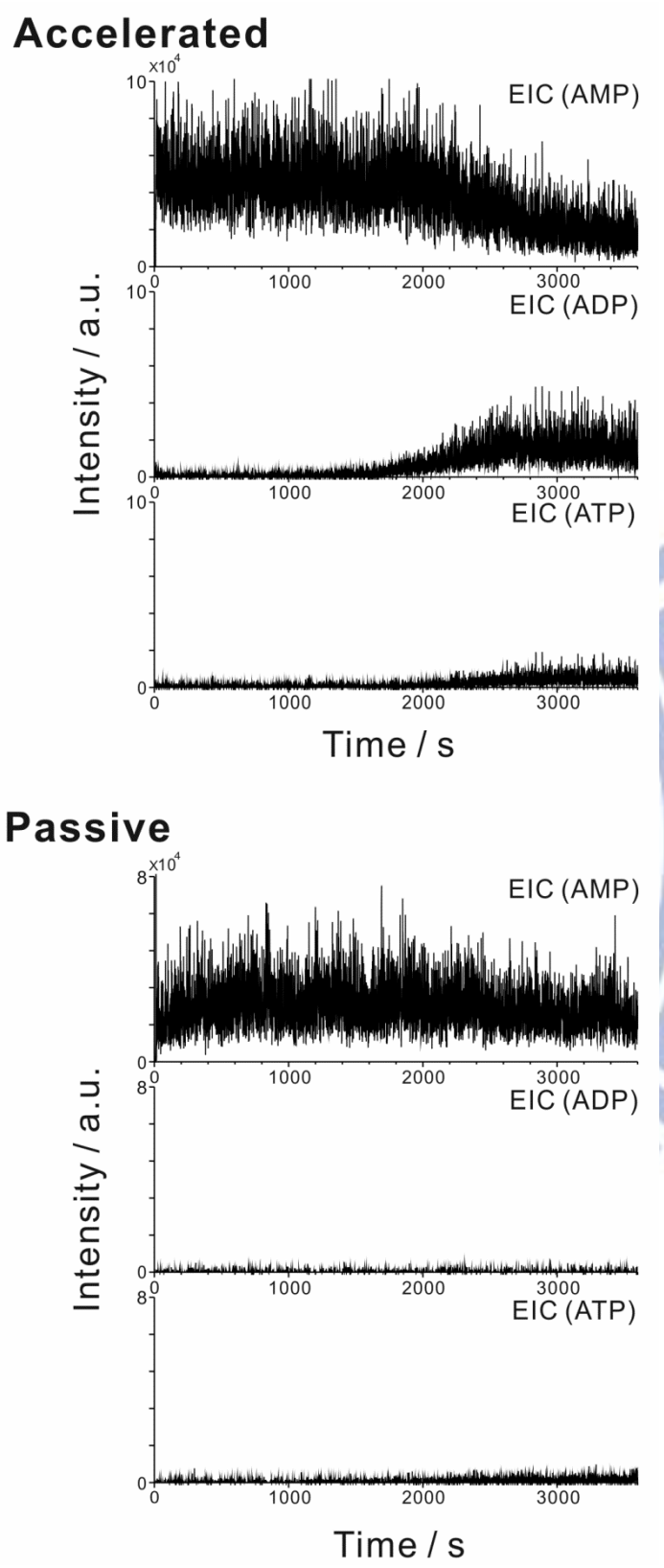

Figure 2.6 Propagation of a bioautocatalytic chemical wave in a horizontal drift cell, recorded online by time-resolved mass spectrometry. Raw data (extracted ion currents) obtained in the same experiment as the one illustrated in **Figure 2. 3**.

2.3.2. Implementation of an isotopically labeled trigger

In order to provide a solid evidence for the higher speed of enzyme-accelerated transduction relative to passive transduction – and overcome the reproducibility problems mentioned above – we subsequently implemented isotopically labeled ATP as a trigger of the chemical wave. When 30 μL $^{13}C_{10}$-ATP is injected to the inlet port of the 600 μL section of the drift cell, it initiates the bienzymatic autocatalytic process. However, since the substrate AMP (0.1 mM) contains ^{12}C isotope, the newly produced ADP and ATP molecules are not labeled. Thus, we can consider the chemical wave produced by the reaction as a carrier of unlabelled ADP and ATP. The labeled $^{13}C_{10}$-ATP migrates mainly due to passive transduction (convection, diffusion, advection (bulk movement of substance due to flow of fluid)), and its role as the reaction trigger ceases as populations of the newly synthesized unlabelled ADP and ATP molecules grow. In this experiment, following the injection of 10^{-2} M $^{13}C_{10}$-ATP, the two waves – corresponding to unlabelled and labelled ADP/ATP species – were recorded. Experimental data were treated according to the following formulae:

$$\text{Rel. yield } (^{12}\text{C}) = \frac{I_{\text{ADP}}+I_{\text{ATP}}}{I_{\text{AMP}}+I_{\text{ADP}}+I_{\text{ATP}}+I_{13\text{CAMP}}+I_{13\text{CADP}}+I_{13\text{CATP}}} \quad \text{(eq. 2.4)}$$

$$\text{Rel. yield } (^{13}\text{C}) = \frac{I_{13\text{CADP}}+I_{13\text{CATP}}}{I_{\text{AMP}}+I_{\text{ADP}}+I_{\text{ATP}}+I_{13\text{CAMP}}+I_{13\text{CADP}}+I_{13\text{CATP}}}, \quad \text{(eq. 2.5)}$$

smoothed, normalized, and displayed in time domain (**Figure 2.7**). The normalization was done by scaling the values of the data points to the maximal value within the displayed time range. Interestingly, even at the high concentration of the trigger ATP (10^{-2} M), a difference in the propagation speed could be observed (**Figure 2.7**, top). In this particular experiment, accelerated transduction led to a sharp increase of the signal (blue trace), whilst passive transduction of labeled ATP led to a gradual increase of the ionizable species (red trace). At a lower concentration of the ^{13}C-ATP, used as the trigger, the edges of the accelerated and the passive fronts were less sharp (**Figure 2.7**, bottom) but the difference between half-maxima of the normalized profiles was greater: 740 *vs*. 93 s in the case of 5×10^{-3} and 10^{-2} M trigger, respectively (**Figure 2.7**). The differences between the accelerated and the passive transduction could be observed in all the replicate experiments using isotopically labeled trigger (**Figure 2.8**) even though both fronts shifted due to the above-mentioned imperfections of the experimental setup. Based on this, one may conclude that – in the present experimental setup – the onset of the increase is determined by the advective transport, and the chemical

wave has a relatively small influence when compared with the advection. It is also worthwhile noting that the inspection of the unnormalized datasets also led to the observation of a higher speed of the bioautocatalytic chemical wave, as compared with the passive transduction (**Figure 2.9**). Nonetheless, the difference is less evident than in the plot of the normalized data (**Figure 2.7**).

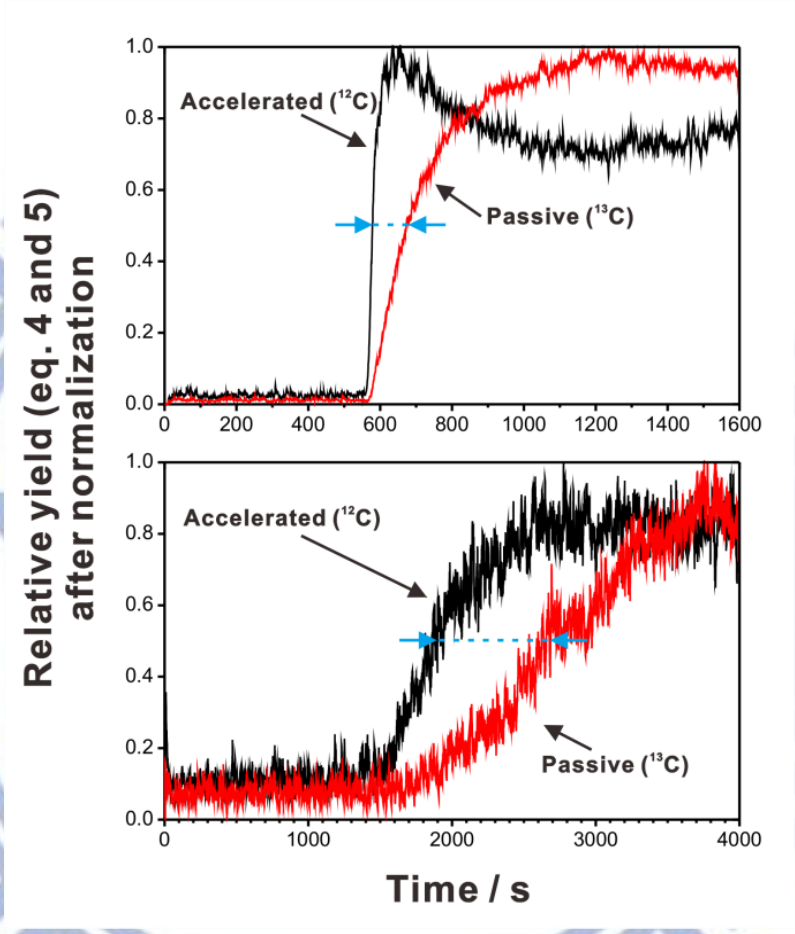

Figure 2.7 Transduction of labelled and unlabelled ATP along the drift cell. Concentration of the $^{13}C_{10}$-ATP trigger: 10^{-2} M (top) and 5×10^{-3} M (bottom). See **Figure 2.8** for replicates of the concentration 5×10^{-3} M. **Figure 2.9** presents unprocessed extracted ion currents from the experiment with the concentration 5×10^{-3} M. Exponential smoothing with a time constant of 4.1 s has been applied, and followed by normalization (scaling to the maximal value). Dashed blue line denotes the time lapse between half-maxima of the normalized curves (0.5 level) corresponding to the passive and accelerated chemical transduction: 93 and 740 s in the case of 10^{-2} M and 5×10^{-3} M trigger solution, respectively.

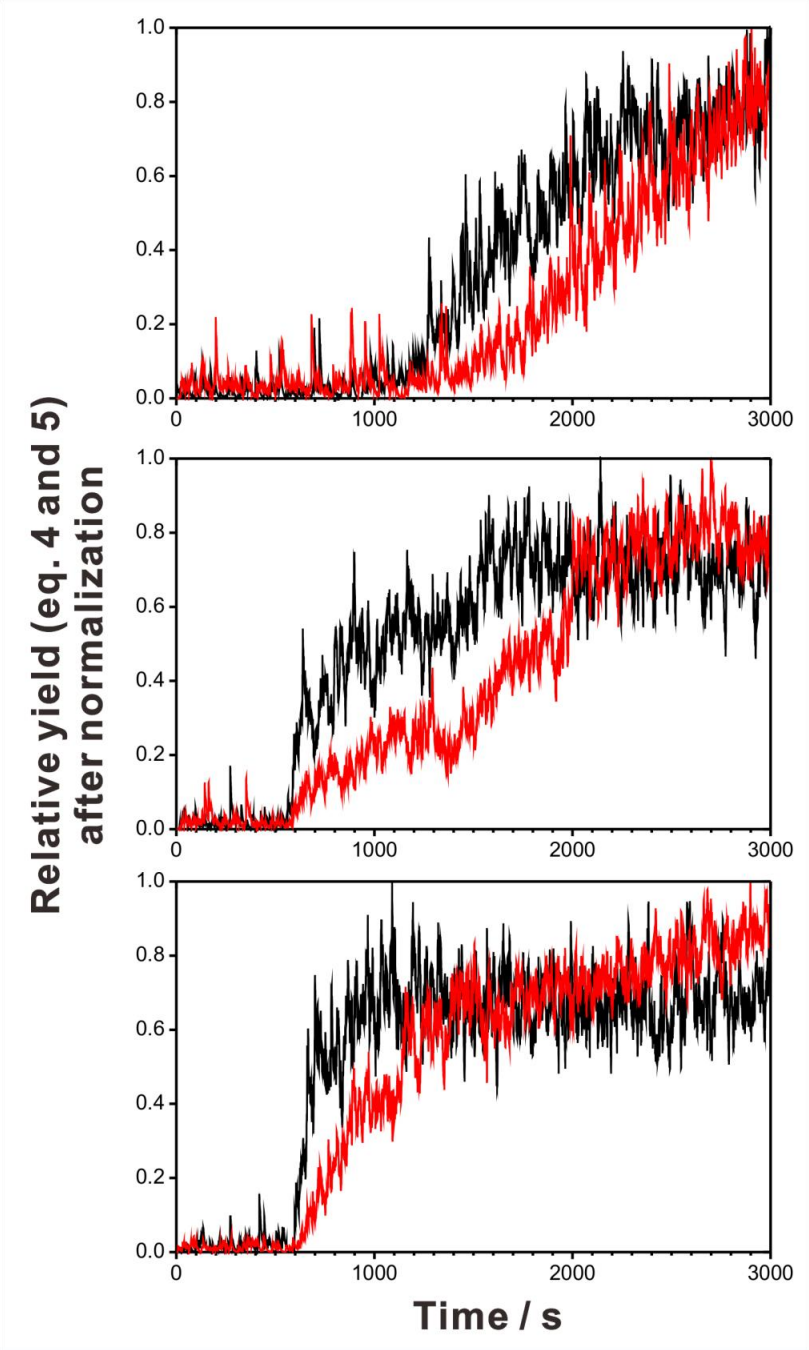

Figure 2.8 Transport of labelled and unlabelled ATP along the drift cell. Concentration of the $^{13}C_{10}$-ATP trigger: 5×10^{-3} M. These three results are replicates of the result shown in **Figure 2.7** (lower panel). Exponential smoothing with a time constant of 4.1 s has been applied, and followed by normalization (scaling to the maximal value).

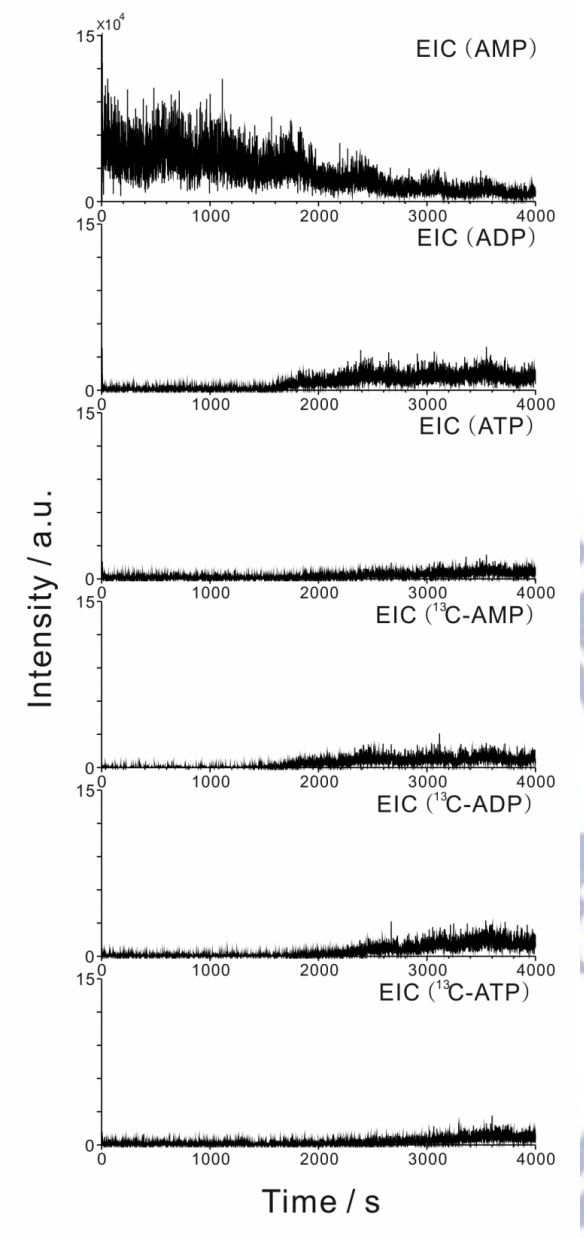

Figure 2.9 Transduction of labelled and unlabelled ATP along the drift cell. Raw data (extracted ion currents) obtained in the same experiment as the one illustrated in **Figure 2.7** (bottom). Concentration of the $^{13}C_{10}$-ATP trigger: 5×10^{-3} M.

2.4. Summary

The results presented above highlight the possibility of using enzyme-aided chemical waves as a means to transmit binary signals. However, to increase practicality of this scheme, one may consider incorporating a "quenching" mechanism, so that the system can return to its initial state (low level of ADP and ATP in the drift cell). This might be achieved by incorporating a mechanism to hydrolyze ADP and ATP to AMP once the signal reaches the

outlet end of the drift cell. It is also worthwhile noting that the experiment using the isotopically labelled trigger ATP does not require additional control because spatiotemporal behaviour of two populations of ATP are recorded in one run.

It was previously reported that hydrodynamic instabilities can be induced by chemical reactions, and subsequently influence convective motion.[58] The current experimental model shows that a chemical reaction itself can produce an apparent "motion" of reactant molecules, which does not seem to be directly connected with advection (that certainly exists in the current experimental system). Chemical waves are often discussed in the context of oscillating reactions, with the most prominent example being the Belousov-Zhabotinsky reaction,[62] which produces oscillating chemical waves composed of iron complexes and other species. Unlike Belousov-Zhabotinsky reaction, the chemical wave reported here has a character of a moving front of elevated concentration, without apparent oscillations (except those attributed to imperfections of the experimental setup and formation of eddy currents). The proposed system is suitable for operation at the room temperature. In addition, unlike many oscillating reaction schemes, the system reported here uses an aqueous buffer at neutral pH, which renders it biocompatible. We believe more chemical wave reaction schemes can be demonstrated in future, for example, implementing various ways of molecular amplification. However, not every amplification reaction can offer the advantage of sending a chemical signal in a seamless fashion. For instance, the most famous one – polymerase-chain reaction (PCR)[63] – requires periodic changes of temperature, which certainly eliminates the advantage of sending chemical signals without the need for actuation by periodic input of thermal energy.

The current results show the possibility to apply time-resolved mass spectrometry in the monitoring of chemical waves. In this demonstration, a relatively low temporal resolution (seconds) was sufficient to observe the between the passive transduction and reaction front. While in previous work we applied optical and mass spectrometric detection in the monitoring of a convection process,[64] here time-resolved mass spectrometry[61] was successfully used to show the difference in the migration speed of chemical waves due to bioautocatalytic reaction and accompanying non-chemical processes.

Modelling biological and chemical processes has been of interest to many scholars. Relevant insights on spatially and temporally resolved processes (such as oscillating reactions) were presented by Arthur Winfree.[65] It might be of potential interest to study the bioautocatalytic process described here in view of the published models of reaction diffusion systems, such as Kolmogorov-Petrovsky-Piskounov's[56] or Fisher's[57] equation. With such

models one could potentially disentangle the contributions of enzymatic reaction and passive dispersion of molecules on the propagation of the moving front of ADP/ATP. However, the current experimental setup has limitations that preclude the use of data in quantitative analysis required to study the mechanism of the chemical wave induced by the bioautocatalytic process. This is due to: (i) the use of an ambient ionization system without separation of analytes; (ii) presence of various components (*e.g.* buffer salt) in the aqueous reaction mixture; (iii) the use of ion trap mass analyzer; (iv) formation of a temperature gradient in front of the mass spectrometer's orifice. Overcoming these drawbacks in future should augment quantitative capabilities of the spatiotemporal monitoring by time-resolved mass spectrometry. However, it is also appealing to implement other detection system when quantitative information is required: for example, fluorescence resonance energy transfer probes, immobilized on the wall of the drift cell. Nonetheless, such optical assays would eliminate the possibility of using isotopic labels to distinguish between the trigger ATP and the ATP produced in the course of the reaction. Therefore, in future studies, it would be interesting to use both mass spectrometry as well as optical detection systems as complementary tools.

In summary, the above results show the possibility of transmitting a chemical signal (ADP/ATP) over the range of centimetres with a speed exceeding that of other transport phenomena occurring under the same conditions. We believe the chemical wave propagating ADP and ATP (the energy carriers in biochemistry) can act as a turn-on/off trigger, and be used to initiate various processes in bioengineered systems incorporating tissues, cells, (bio)nanorobots, or various biocatalysts (*e.g.* kinases). Coupling this scheme with other biomolecular constructs (*e.g.* enzyme systems supplying the AMP and PEP substrates) and microfluidics (*e.g.* parallel capillary channels), and using anti-convective media (*e.g.* hydrogels), may further enable multiplexed transmission of binary data. Since the speed of chemical waves – propagating according to the proposed scheme – is related to the kinetic properties of the enzymes involved in the bienzymatic process (*cf.* **Figure 2.2**), modification of these enzymes (for example, through directed evolution), or taking advantage of non-enzymatic amplification schemes,[66] might further increase the speed of wave propagation, which would augment practicality of this approach for real-world applications.

Chapter 3.

Pinch-valve interface for automated sampling and monitoring of dynamic processes by gas chromatography – mass spectrometry

3.1.Introduction

Assaying enzymatic activity has been an indispensable part of studies in biochemistry and biotechnology.[67-69] Being biocatalysts, enzymes speed up chemical reactions by lowering the activation energy.[70, 71] Enzymes provide improved efficiencies by increasing the reaction rates. Due to their specificity, they ensure high purity of the synthesized products. Appropriate assays need to be developed in order to characterize catalytic properties of enzymes. Ideally, such assays should enable reaction monitoring within certain periods of time, so that any loss of catalytic activity can be easily noted. Due to the high price of enzymes, it is also desirable that these methods consume as little sample (biocatalyst) as possible.[72] As outlined in **Chapter 1**, gas chromatography (GC)-based methods have been in common use since the 1950s.[27, 28, 73] In order to ascertain satisfactory sensitivity and selectivity, high-performance detectors are normally connected to outlets of GC columns. For instance, mass spectrometry (MS) is one of the popular detectors hyphenated with GC systems because it can assist identification of the eluting molecules based on their mass-to-charge ratios (*m/z*) and fragmentation patterns. Owing to their versatility and ruggedness, the hyphenated GC-MS systems are used in routine analyses in environmental science,[74] forensic science,[75] geological sciences,[76] food chemistry,[32] cosmetics[77] and biochemistry[78] – to name just a few application areas.

In general, to obtain high-quality results, and to minimize manual effort, automated sampling devices are combined with GC instruments. Autosamplers make the entire analytical procedure straightforward, and they facilitate high-throughput operation. Clearly, superior repeatabilities can be obtained with robotised autosamplers[79] as compared with the manual injection. GC instruments (sometimes equipped with autosamplers) are often used in discrete analyses – one sample at a time. This mode of operation can provide data on the yield of chemical or biochemical reactions at a given time point.[80, 81] To obtain data revealing progress

of a chemical reaction, aliquots of the reaction mixture are withdrawn from the reaction vessel, and transferred to the GC apparatus.[82] This "low-tech" sampling step conspicuously curtails the advantage of utilizing automated systems since the key part of the analytical procedure (*i.e.* sampling routine) is performed by humans. Moreover, the involvement of manual operation makes it difficult to time the sampling, thus reducing usefulness of the resulting data in post-run kinetic evaluations. Hence, there is a need to develop automated sampling tools which could easily be coupled with inlets of GC instruments, and enable assaying chemical processes in real time. Such systems could provide optimum conditions (*e.g.* temperature control, stirring) for the studies of dynamic processes, and reduce the delay time between sampling and analysis.

Microcomputers and microcontrollers are vital for the construction of analytical instrumentation.[83, 84] In fact, most commercial instruments incorporate customized microcontroller circuits. In the past few years, many universal microcontrollers have become available. One prominent example is the Raspberry Pi – a single printed circuit board (PCB) microcomputer, which was introduced to the market in 2012.[85, 86] The original purpose of the Raspberry Pi was to enhance education in computer science, electronics, automation, and robotics.[87] Plethora of practical uses of this universal platform have emerged soon after the sales had started.[88] Typical applications include: data logging, sensing, controlling displays, and automation of household appliances.[89] The introduction of the Raspberry Pi – as well as other platforms such as Arduino,[90] Netduino,[91] mbed,[92] or Beaglebone[93] – has inspired home-grown innovators, and fostered creativity of students. These versatile and easy-to-use electronic circuits nowadays find applications in scientific instrumentation, including the construction of analytical systems.[94-96] In this study, we aimed to develop a facile automated injection system for GC to accommodate monitoring of dynamic samples, which would incorporate minimum number of mechanical parts, and be controlled by the Raspberry Pi microcomputer. The system comprises control panel, peristaltic pump, two pinch valves, and GC-MS apparatus (**Figure 3.1**). We further demonstrate the applicability of this system in the monitoring of transesterification reaction catalysed by single microbeads containing immobilised lipase enzyme as well as extraction of natural products from small amounts of plant tissues.

3.2. Experimental section

3.2.1. Samples and chemicals

A widely available thermostable recombinant lipase (from *Candida antarctica*, expressed in

Aspergillus niger; E.C. 3.1.1.3) adsorbed on macroporous acrylic resin (specific activity: ≥ 5,000 U g^{-1}, microbeads) was used as the main model sample (*cf*. section **3.3.3.**). The samples of lemon and kumquat (*cf.* section **3.3.4.**) were obtained from local grocery shops. Small fragments (~ 2 mm, < 5 mg) of the fruit peel were obtained using stainless steel blade. Isopropenyl acetate, LC-MS grade acetonitrile, D-limonene, β-pinene, γ-terpinene, and thymol were all purchased from Sigma-Aldrich (St Louis, MO, USA). 1-Butanol was purchased from Merck (Darmstadt, Germany).

3.2.2. Interface

The interface comprises a Y-junction (P-779, PEEK NanoTight Union, OD 1/16-inch; IDEX Health & Science, Oak Harbor, WA, USA) and two solenoid pinch valves (12 V DC, P/N 075P2NO12-01S and P/N 075P2NC12-01S; Bio-Chem Fluidics, Boonton, NJ, USA): out of which one is "normally closed" (NC) while the other one is "normally open" (NO; **Figure 3.1**). The valves were attached onto a flat support made of 1-cm-thick plywood with plastic holder and a small amount of modelling clay (Sugru; FormFormForm, London, UK), supported by four stainless steel breadboard-type posts (TR75/M-P5, ∅ 1.2 cm, 7.5-cm long). The sample was delivered by a peristaltic pump (Ismatec ISM936D, IPC Series, 8 channels; IDEX Health & Science). The pump pushed the liquid along a 35.4-cm-long section of Tygon tubing (ID 0.25 mm, OD 2.07 mm, cat. No. SC002; IDEX Health & Science), connected to a 28.6-cm-long section of polytetrafluoroethylene (PTFE) tubing (OD 1.58 mm, ID 0.3 mm,cat. No. 58702; Supelco, Bellefonte, PA, USA), and – further downstream – to the Y-junction (via a 4.8-cm-long section of polyimide-coated fused silica capillary; ID 150 μm, OD 375 μm, cat. No. 1010-32132; GL Sciences, Tokyo, Japan). The other port of the Y-junction was connected (via another 4.8-cm-long section of polyimide-coated fused silica capillary, 15-cm section of PTFE tubing, and a 31.4-cm-long section of silicone tubing) to the NO pinch valve. The outlet end of the silicone tubing – passing the pinch valve – was dipped into the waste collector (20-mL glass vial). The outlet port of the Y-junction was connected via a 6-cm-long section of silicone tubing to a 1/16-inch union (IDEX Health & Science). The other side of this union was fitted with a metal needle removed from a discarded solid-phase microextraction (SPME) fibre assembly (23 ga, cat. No. 57284-U; Supelco). The NC pinch valve was mounted on the 6-cm silicone tubing joining the Y-junction and the 1/16-inch union. While on stand-by, the liquid – delivered by the pump – was directed to the waste reservoir because the NC pinch valve prevented its entry to the stainless steel needle. However, when the NC valve got open, and the NO valve got closed, the liquid was directed towards the metal needle, and further on

to the injection port of the GC instrument.

The sample vial was placed inside a small thermoshaker (Vortemp 56 EVC; National Labnet Company, Woodridge, NJ, USA) to assure optimum conditions for the studied process (*e.g.* reaction, extraction). To ascertain seamless operation of the system it is recommended that the Tygon tubing is replaced every day, and the system rinsed before operation with the solvent used in the analysis for ≥ 15 min. Note that the room temperature during the experiments described here was ~ 20 °C; it is expected that huge variations of ambient temperature could potentially affect reproducibility of the described method.

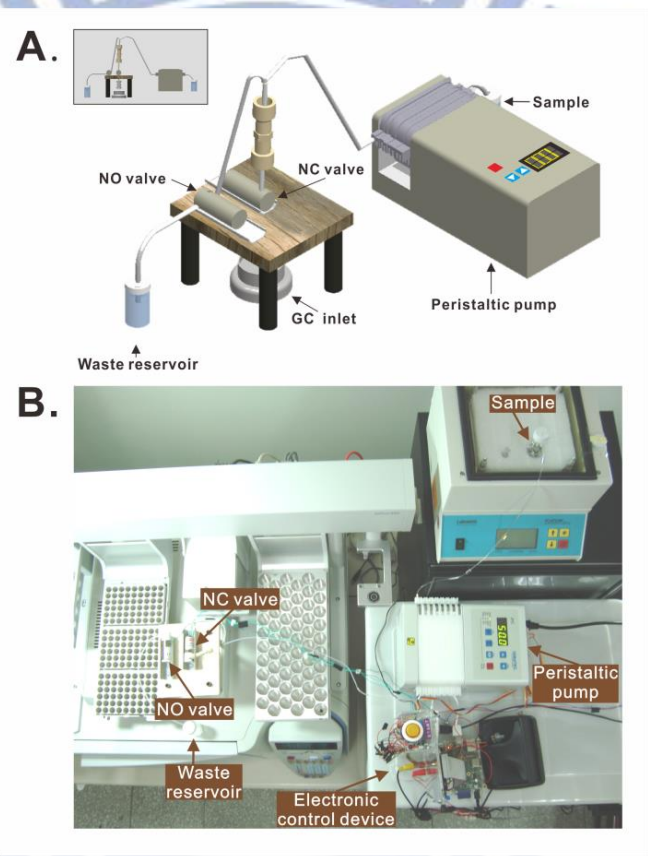

Figure 3.1 System for online sampling and sample introduction to gas chromatography – mass spectrometry using pinch valves: (A) device layout; (B) view of the assembled device. NO – normally open valve. NC – normally closed valve. Note well: The commercial autosampler (left-hand side) was not used in this study. The lid of the mini-thermoshaker (upper right-hand side) was closed during the experiment.

3.2.3. Electronic control system

In order to control operations of the on-line GC-MS injection system, we implemented a single board microcomputer – Raspberry Pi (Type B) with a 700-MHz central processing unit (ARM1176JZF-S) and 512-MB random-access memory (**Figure 3.2**). It was set up with a

Linux-related operating system (Debian/Raspbian Wheezy, 2012) loaded from an 8-GB secure digital (SD) memory card (Transcend, Taiwan). The microcomputer was connected to a multifunction input/output extension PCB (Pi PLUS; web4robot.com, Parkville, MD, USA) via its general-purpose input/output (GPIO) interface to facilitate sending out digital control signals, and further development of the system. For convenience of operation and programming, it was also fitted with standard peripherals (keyboard, mouse, WiFi dongle) and a miniature (~ 4.4 inch) liquid crystal display (LCD) monitor (connected to the RCA-type port of the Raspberry Pi PCB). The control program – written in C – was referenced to the Pi PLUS function codes and header files provided by the manufacturer (web4robot.com), compiled with the GNU compiler on the Raspberry Pi, and deployed. The "sleep()" command was used to time the injection. The Pi PLUS extension PCB was connected via digital interface pins to three relay boards (2 relays each; Songle Relay, Ninbo, China). The relays controlled the main functions of the system – including peristaltic pump (on/off, change of direction), operation of the pinch valves, and sending a trigger signal to the GC-MS instrument. All the PCBs and the monitor were fitted into an acrylic stand (Muji, Tokyo, Japan). The device also featured a "START" button which activated the functions of the program. The flow rate was regulated by adjusting the electric potential on the pin No. 5 of the peristaltic pump interface – this was enabled by a 50 kΩ potentiometer (R_{POT}) in a voltage divider circuit (**Figure 3.2**). For convenience, and to avoid electrical interferences, the main components were powered from separate power supplies – Raspberry Pi: 5 V, 1 A; Pi PLUS: 9 V, 1.3 A; pinch valves: 12 V, 1.5 A; monitor: 9 V, 1 A.

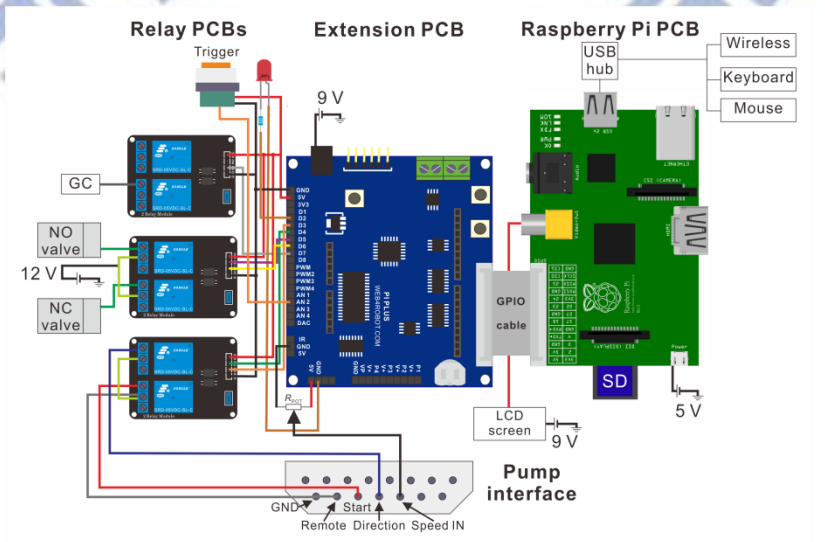

Figure 3.2 Layout of the electronic connections of the device microcontroller unit incorporating the Raspberry Pi microcomputer, general purpose input / output extension board, and relay boards.

3.2.4. Apparatus and method

The testing as well as the subsequent analyses were performed using a commercial gas chromatograph (TRACE GC; Thermo Fisher Scientific, Waltham, MA, USA) coupled with a single quadrupole mass spectrometer (ISQ; Thermo Fisher Scientific). Capillary column with non-polar phase comprising 5% phenyl methyl polysiloxane (TRACE SPB-5; length: 60 m; ID 0.53 mm; film thickness: 1.5 μm) was used. The eluting compounds were ionized by EI source operating at 70 eV. Internal calibration of the mass spectrometer was conducted using perfluorotributylamine (Alachua, FL, USA). Helium gas was used as the mobile phase with the constant flow rate of 1 mL min^{-1} at a pressure of 10 kPa. The injector was kept at 280 °C. Split injection was used with the split ratio of 50. In the first part of the study (enzymatic reaction), the following separation conditions were used: Column temperature was initially set to 40 °C. Following 3 min of separation, the temperature was gradually increased reaching 60 °C after 2 min (ramp: 10 °C min^{-1}), then increased to 100 °C (ramp: 35 °C min^{-1}). In the final stage of the run, temperature was increased to 150 °C (ramp: 20 °C min^{-1}). It was kept constant for 5 min (till the end of the analysis). The mass spectrometer was set to record ions in the range of 42-250 u e^{-1}. The analyte (butyl acetate) species were monitored at the *m/z* 43 u e^{-1}while the internal standard (limonene) species were monitored at the *m/z* 93 u e^{-1}. In the second part of the study (extraction of plant tissue samples), the following separation conditions were used: Column temperature was initially set to 40 °C, and after 3 min, the temperature was increased to 120 °C (ramp: 30 °C min^{-1}). Subsequently, temperature was increased up to 180 °C (ramp: 15 °C min^{-1}), and it was kept constant for 7 min (till the end of analysis). In this experiment, the mass spectrometer was set to record ions in the range of 40-250 u e^{-1}. The analyte (limonene, pinene, terpinene) species were monitored at the *m/z* 93 u e^{-1}while the internal standard (thymol) species were monitored at the *m/z* 135 u e^{-1}.

3.2.5. Data treatment

The data were acquired using the Xcalibur software (ver. 2.1.0 SP1.1160; Thermo Fisher Scientific), and saved in the ".raw" files. The raw data (extracted ion currents, EICs) were copied from the Xcalibur software (ver. 2.1.0 SP1.1160, Qual Browser) to Excel software (ver. 2010; Microsoft, Redmond, WA, USA), and imported to PeakFit (ver. 4.12; SeaSolve

Software, San Jose, CA, USA) for further analysis. The linear baseline was typically fitted according to the 2-point criterion. Fast Fourier transform filter (10-25%) was normally applied. The peaks were fitted using the Gaussian or the Haarhoff – Van der Linde function. The final values were computed using Excel, and then the data were transferred to Origin (ver. 8.0724; OriginLab, Northampton, MA, USA) for final display.

3.3. Results and discussion

3.3.1. Construction of the automated pinch-valve sampling system

When designing the automated device for sampling dynamic chemical processes prior to the analysis by GC-MS, we were inspired by the work conducted by Quintana and co-workers[97] who developed an ingenious lab-on-valve system for determination of polychlorinated biphenyls incorporating GC apparatus as a detection tool. In another noteworthy study, Clavijo *et al.*[98] developed a lab-on-valve microextraction system coupled with GC-MS for the determination of polycyclic aromatic hydrocarbons in water. Their automated system showed good precision in quantitative analysis (relative standard deviation (RSD) < 5%). In the current study, it was of paramount importance to take into account the compatibility of the chemical process to be assayed and the analytical requirements. It was crucial that the studied process could be conducted at preset and constant temperature with shaking/stirring. It was also necessary to make the transfer line as short as possible to reduce the delay time between the sample collection and injection. Finally, it was vital that a defined aliquot of the sample could be introduced to the injection port of GC apparatus at pre-defined time points. At the same time, unlike in the work by Quintana and co-workers,[97] here it was not critical to conduct sample preconcentration, which would inevitably slow down the analysis of the consecutive sample aliquots obtained from a dynamic system (*e.g.* reaction mixture).

In the final version of the system, we used polymer (Tygon, silicone, PTFE) and silica tubing to aspirate small aliquots of the studied medium and transfer them hydrodynamically to the injector of the GC-MS instrument. The hydrodynamic flow was exerted by a peristaltic pump. The Reynolds numbers along the flow line are in the order of 10-20 (as calculated for 100% acetonitrile), which points to predominance of laminar flow in the sample conduit. Directing the sample to the GC injector was facilitated by two pinch valves (NO and NC; **Figure 3.1**). Efficient control of the flow was achieved by means of the electronic

microsystem triggering five relays (see section **3.2.3.**, **Figure 3.2**). All the operations of the system were programmed in a C-language script, and executed according to the optimized time schedule (**Table 3.1**). After setting up, the operation of the system was triggered by pressing a single button (**Figure 3.2**). The samples were then injected, and GC-MS signals were automatically recorded and saved in a sequence for post-run processing. The seamless operation of the system significantly minimized the extent of mechanical and manual tasks to be performed during the analysis.

3.3.2. Characterization of the automated pinch-valve sampling system

Figure 3.3 and **Table 3.1** present the operation steps of the pinch valves during sample injection. In a nutshell, the 1st step encompasses withdrawal of an aliquot of the liquid sample from the sample chamber. During this step, the transfer tubing is filled with a fresh portion of sample, and any excess sample is diverted to waste. Considering the applied flow rate (1.25 µL s^{-1}) and the sampling time (79 s; **Table 3.1**), the volume of sample withdrawn in this step is estimated to be ~ 99 µL. In the 2nd step, the sample is directed to the injection port of the GC apparatus during 28 s, which contributes to the withdrawal of further ~ 35 µL of sample from the sample vial. Eventually, in the 3rd step, the sample is pushed out toward the liner during 6 s, which adds ~ 8 µL to the volume of sample aspirated by the sampling capillary (see the following paragraph for further discussion of the injection volume). In the 4th step, ~ 50 µL of the "old" sample are returned to the sample chamber, and a small volume of fresh sample (5th step: 15 s, ~ 19 µL) is immediately introduced to the flow line. Therefore, ~ 111 µL of the sample solution are consumed in every analysis, most of which is discarded to waste, only a small fraction being dispensed to the GC column inlet. The purpose of withdrawing larger sample volumes than it is actually needed for analysis is to rinse away any residues of the previously analysed sample aliquots from the system. It should be borne in mind that although the 3rd step consumes ~ 8 µL of sample, less sample may actually be introduced to the cavity of the GC liner. This is because the distal part of the needle is believed to be filled with pressurised gas after the completion of the 3rd step. In fact, this might help to avoid premature injection of the sample present in the needle due to thermal expansion of solvent at elevated temperature.

Several experiments were conducted to verify injection accuracy and precision of the proposed device. In an offline experiment, an analytical balance was used to determine the

total mass of the sample (acetonitrile : 1-butanol : isopropenyl acetate = 90 : 9 : 1 (v/v/v)) aliquot pushed out from the needle tip. The obtained value was 7.2 ± 1.7 mg (SD, n = 10) which corresponds to 9.2 ± 2.2 μL (d = 781 kg m^{-3}), and remains in a good agreement with the value predicted above. The obtained RSD in the injection repeatability test – conducted at ambient conditions (temperature: ~ 20 °C; atmospheric pressure: ~ 101 kPa) is satisfactory (24%; n = 10). However, one shall not exclude a possible influence of the GC operating conditions (temperature inside the liner: 280 °C; pressure in the injector: 10 kPa) on the injection. Therefore, we also evaluated repeatability of the operation of the automated device after coupling it with the GC-MS instrument (**Figure 3.1**). The RSD of the peak areas of a test analyte (1-butyl acetate in the mixture: acetonitrile : 1-butanol : isopropenyl acetate = 90 : 9 : 1 (v/v/v)) recorded during 10 consecutive runs was 27%. When considering the peak areas of the test analyte referenced to an internal standard (D-limonene), the RSD decreased to 13% (**Figure 3.4**, EICs for analyte, *m/z* 43 ± 0.5 and internal standard, *m/z* 93 ± 0.5 u e^{-1}); this was deemed acceptable for further applications. To measure the accuracy of the digital control of sample injection connected to electromechanical actuators (relays, pinch valves), we carried out the following experiment: a video/audio sequence was recorded to capture the action of the relays and the acoustic sounds produced by the relays and the pinch valves. Using a video/audio processing software (Ulead Video Studio, ver. 10.0.0110.0 SE DVD; Ulead Systems, Taipei, Taiwan), we estimated the time gaps between the acoustic signals marking the beginning and the end of the injection. The average interval between the "clicks" of the pinch valves was estimated to be 6.0 ± 0.0 s (n = 3). Considering that the injection time was set to 6 s (in the programme loaded into the Raspberry Pi microcomputer), this result shows that the proposed device provides an accurate and precise control over the injection time. However, other sources of inaccuracy and imprecision exist; they are believed to be related to the mechanic actuation of the peristaltic pump, tube plasticity, and other causes. In another experiment, we estimated the actual injection volume obtained when the automated injection system was coupled with the GC-MS apparatus (**Figure 3.5**): 1.7 ± 0.4 μL (n = 3; based on comparison of peak area obtained using the automated system with the peak areas obtained by performing manual injections of different volumes of the standard sample). We think that the lower injection volume in this on-line experiment is due to the influence of gas pressure (10 kPa) inside the liner of the GC-MS instrument. It can be concluded that although the RSDs observed in this study were slightly higher than those obtained with lab-on-valve systems, the injection repeatability can be regarded as satisfactory. In order to bring the RSD

values down, and obtain reliable analytical data, it is certainly required to use internal standards (spiked to the samples).

To further characterise the performance of the automated sampling/analysis system (**Figures 3.1** and **3.2**), we verified its quantitative capabilities. **Figure 3.6** presents calibration plots for 1-butyl acetate, D-limonene, β-pinene, and γ-terpinene. All these compounds are relevant considering the foreseen applications of the system (see sections **3.3.3.** and **3.3.4.**). The coefficients of determination in these plots are within the range: 0.944 – 0.989 (**Table 3.2**); which is believed to be acceptable for the anticipated applications. The increased standard deviation – observed at higher concentration values (**Figure 3.6**) is believed to be caused by inaccuracy of curve fitting while measuring areas of highly deformed peaks. The range of the assay was narrowed down to maintain the coefficients of determination at a high level (> 0.9; **Table 3.2**).

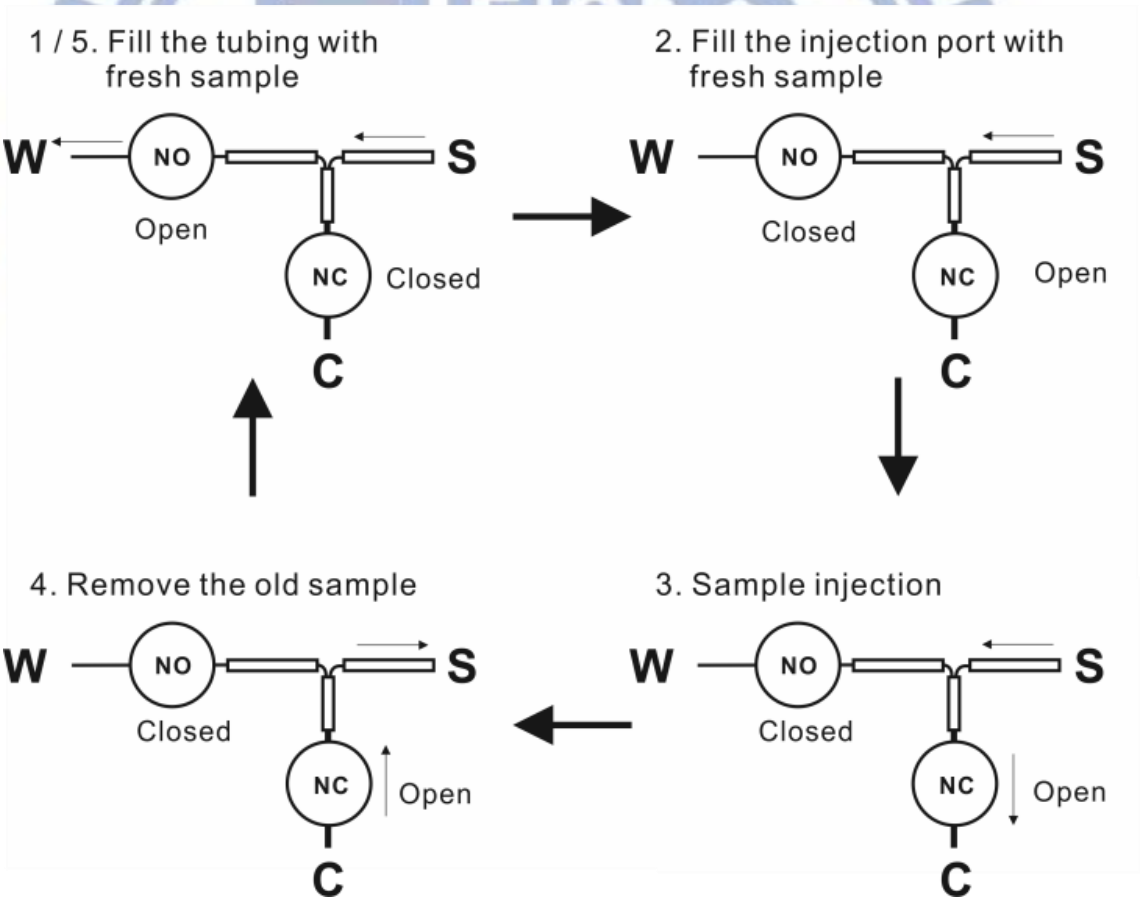

Figure 3.3 Schematic diagram of the injection sequence executed using the automated device (*cf.* **Figures 3.1** and **3.2**) incorporating two pinch valves (NO – normally open; NC – normally closed). Labels: S – sample, W – waste, C – column.

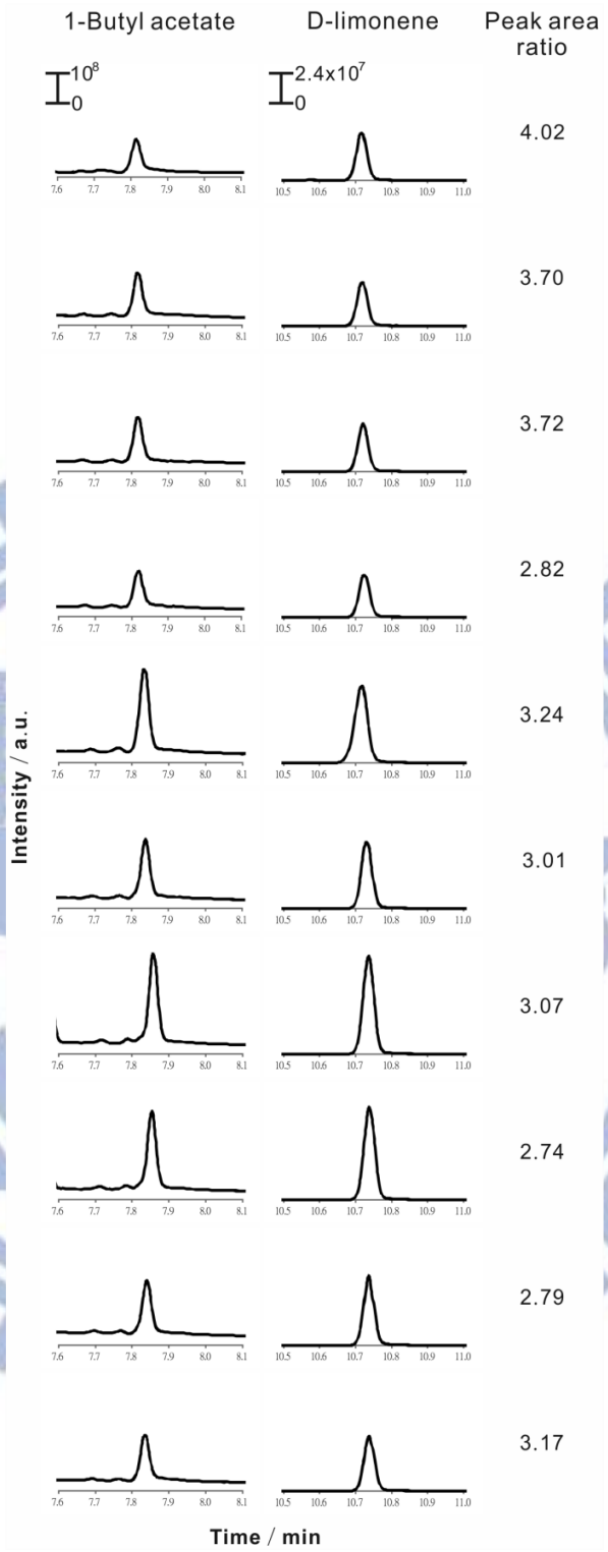

Figure 3.4 Injection repeatability test. EICs (analyte *m/z* 43 ± 0.5 u e^{-1}, internal standard *m/z*, 93 ± 0.5 u e^{-1}) from 10 consecutive analyses carried out using the automated sampling system (**Figures 3.1** and **3.2**) combined with GC-MS instrument. Sample: 86.1 μM 1-butyl acetate, 36.7 μM D-limonene (in acetonitrile).

Table 3.1 Operation sequence of the custom device for the introduction of liquid samples to the injector of gas chromatography apparatus using pinch valves.

Operation	Step (*cf*. Figure 3.3)	Duration / s	Direction of flow	Normally closed (NC) valve (ON / OFF)	Normally open (NO) valve (ON / OFF)
Fill tubing (Tygon and PTFE between the sample chamber and the injection port) with fresh sample	1	79	Normal	OFF	ON
Fill the injection port with fresh sample	2	28	Normal	ON	OFF
Injection	3	6	Normal	ON	OFF
Remove old sample from the injection port	4	40	Reverse	ON	OFF
Push old sample to the waste reservoir	5	15	Normal	OFF	ON

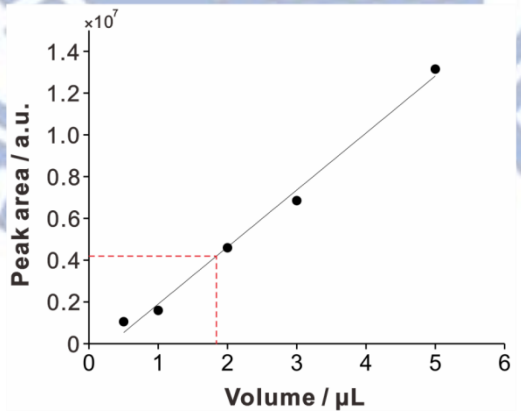

Figure 3.5 Determination of the injection volume using the automated sampling/injection system. The black solid markers correspond to the manual injections (without the automated system). The black solid line is a linear function fitted to those data points. The red line extrapolates the peak area (EIC analyte *m/z* 43 ± 0.5 u e^{-1}, internal standard *m/z*, 93 ± 0.5 u e^{-1}) obtained with the automated injection system (n = 3) to the volume axis. The concentration of the 1-butyl acetate standard was 0.5 µM in both cases. Each data point in this graph corresponds to arithmetic average of two replicate results.

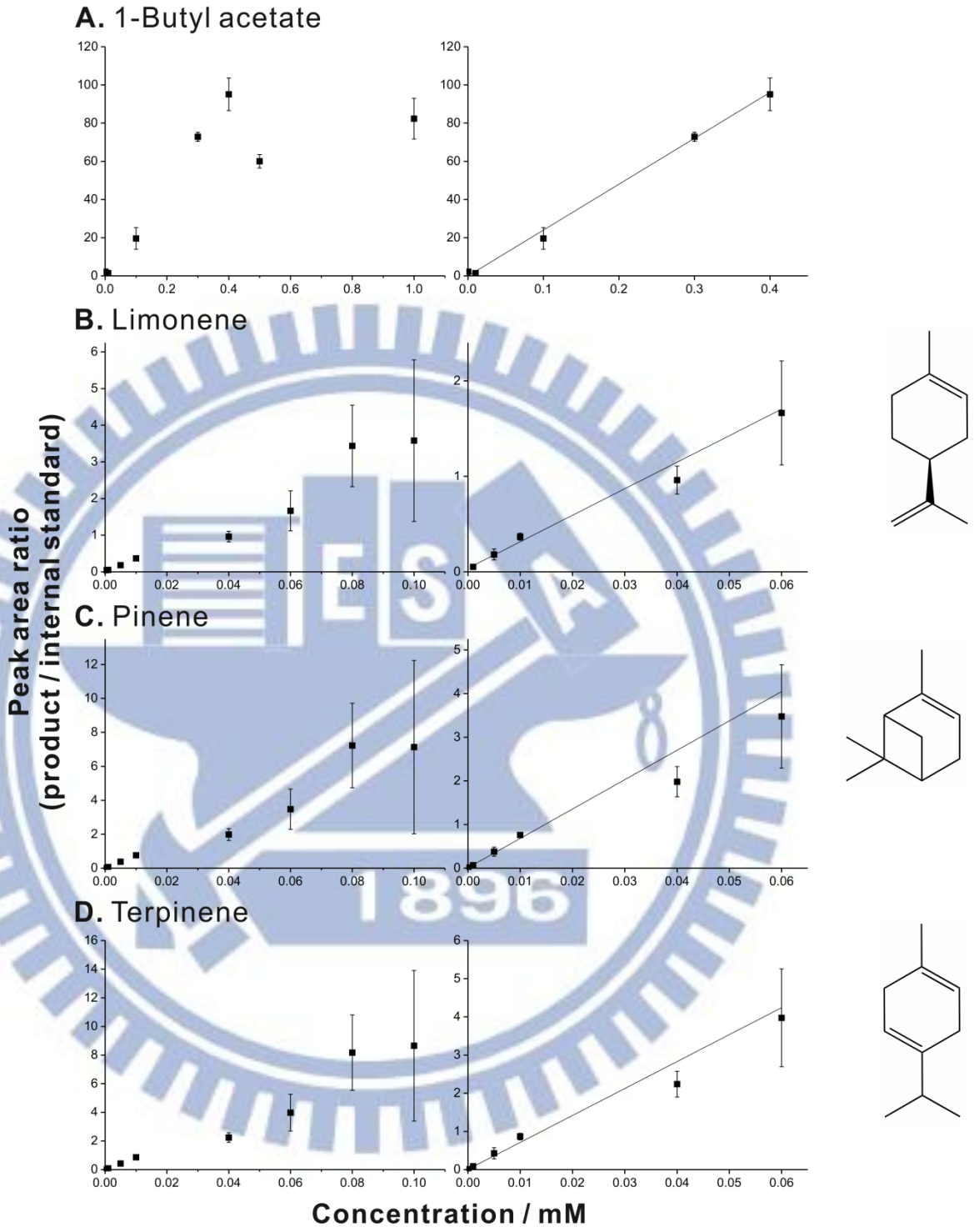

Figure 3.6 Quantitative capabilities of the proposed automated sampling system (**Figures 3.1** and **3.2**) coupled with GC-MS. (A) Calibration plot for 1-butyl acetate (D-limonene as internal standard). (B) Calibration plot for D-limonene, (C) β-pinene and (D) γ-terpinene (thymol as internal standard). Error bars correspond to standard deviations (n = 3). For calibration equations, see **Table 3.2**

Table 3.2 Calibration equations (*cf.* **Figure 3.6**) and limits of detection (LODs) for the four analytes discussed in this report. The LODs were calculated using the $S/N = 3$ criterion, where S is the peak amplitude and N is the RMS noise of baseline. The injection volume resulting from the estimation described in section **3.3.2.**was used to calculate $LOD_{tot.}$. Note well, the conditions used to analyse the first (1-butyl acetate) and the other three (limonene, pinene, terpinene) compounds are different (*cf.* section **3.2.4.**).

Compound	**EIC (*m/z*, range) / u e^{-1}**	**Ret. time / min**	**Internal standard (IS)**	**EIC of IS (*m/z*, range) / u e^{-1}**	**Ret. time of IS / min**	**Calibration equation** ***A*** **– area ratio (analyte/IS)** ***C*** **– concentration / mM**	**Coefficient of determination (R^2)**	**Linear range / mM**	**$LOD_{conc.}$ / mM (± SD, *n* = 3)**	**$LOD_{tot.}$ / mmol (± SD, *n* = 3)**
1-Butyl acetate	43 ± 0.5	7.9	10^{-5} M limonene	93 ± 0.5	10.7	$A = (240.3\pm7.8)C - (0.0550\pm0.5481)$	0.989	0.0005-0.0400	1.97×10^{-4} $\pm2.48\times10^{-5}$	3.34×10^{-10} $\pm4.21\times10^{-11}$
Limonene	93 ± 0.5	9.3	10^{-5} M thymol	135 ± 0.5	12.4	$A = (27.8\pm2.9)C + 0.0373\pm0.0198)$	0.944	0.0001-0.0600	2.96×10^{-5} $\pm6.89\times10^{-6}$	5.03×10^{-11} $\pm1.17\times10^{-11}$
Pinene	93 ± 0.5	8.9	10^{-5} M thymol	135 ± 0.5	12.4	$A = (67.3\pm4.4)C + (0.00830\pm0.00510)$	0.965	0.0001-0.0600	1.50×10^{-4} $\pm5.93\times10^{-5}$	2.55×10^{-10} $\pm1.01\times10^{-10}$
Terpinene	93 ± 0.5	9.6	10^{-5} M thymol	135 ± 0.5	12.4	$A = (70.6\pm5.7)C + (0.00660\pm0.00490)$	0.949	0.0001-0.0600	9.66×10^{-5} $\pm1.92\times10^{-5}$	1.64×10^{-10} $\pm3.26\times10^{-11}$

3.3.3. Application in the monitoring of single-microbead biocatalysis

While many assays for lipases (*e.g.* spectrophotometry-based)[99] focus on the hydrolytic activity of these enzymes,[100] for practical applications it is desirable to probe their transesterification activity.[72, 101] Therefore, to exemplify capabilities of the proposed automated system (**Figures 3.1** and **3.2**) in bioanalysis, first we applied it in the monitoring of a transesterification reaction catalyzed by lipase immobilized on macroporous resin microbeads:

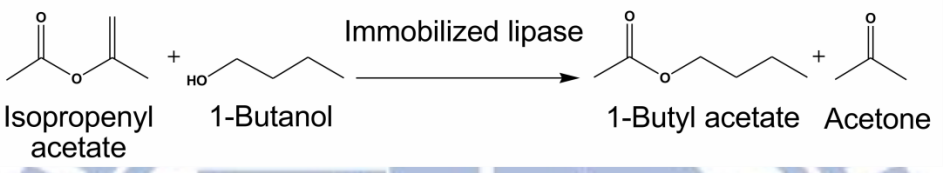

(eq. 3.1)

It should be noted that transesterification is a crucial step in the production of biodiesel fuel; therefore, it is of considerable relevance when it comes to harnessing green energy.[16] From the model transesterification reaction depicted in eq. 3.1, it is evident that transferring acyl group from isopropenyl acetate onto the molecule of 1-butanol leads to formation of a new ester (1-butyl acetate) and a by-product (acetone). Using the GC method described in section **3.2.4.**, it is possible to separate 1-butyl acetate from all other components of the reaction mixture (**Figure 3.7**)

We further applied the proposed system in the monitoring of transesterification catalyzed by varied numbers of lipase microbeads (n = 1, 2, 3, 4, 5, and 10). As expected, the enzyme progress curves obtained for different numbers of microbeads have different slopes (**Figure 3.9**). Following 126-min incubation, the relative reaction yield – as expressed by the ratio of the product 1-butyl acetate area *vs.* the internal standard (D-limonene) peak area – recorded for 10 enzyme microbeads – is highest (**Figure 3.9**, dark blue diamonds). Notably, the relative reaction yield – recorded for 1 enzyme microbead (**Figure 3.9**, red circles) – is only slightly higher than the blank (reaction mixture incubated without biocatalyst microbeads; **Figure 3.9**, black triangles). Nonetheless, it is pleasing to note that the amount of product, obtained in the presence of individual microbeads, is detectable. Motivated by this success, we carried out a comparative study of biocatalytic performance of single enzyme microbeads. As shown in **Figures 3.8** and **3.10**, the activities of individual microbeads (n = 8) are not exactly the same. The reaction velocities (calculated by fitting linear functions to the data sets in **Figure 3.10**

and feeding the slopes into the calibration equation from **Table 3.2**) range from 308 to 432 nmol L^{-1} min^{-1} (**Table 3.3**).

Note well that the 126-min period corresponds to the initial stage of reaction since the concentration of isopropenyl acetate is in the order of ~ 0.1 M, and only few percent of it are depleted (assuming 1:1 reaction stoichiometry, eq. 1). Interestingly, there is no evident correlation between the relative reaction yields (for the 126 min time point) and the specific dimensions of the studied microbeads (diameter, outer surface area, volume; **Figure 3.11**). In fact, one outlier point in **Figure 3.11** indicates the incidence of particularly large microbeads with disproportionately low enzymatic activity within the microbead population. This unexpected result can be explained with the anticipated heterogeneous immobilization of lipase molecules on the surface of the acrylic resin. This observation was only possible when conducting single-microbead assay. It can be of use whenever it is required to probe transesterification activities of very small samples of heterogeneous biocatalysts. The heterogeneity of lipase microbeads indicates that multiple microbeads need to be tested one-by-one before a conclusion on the overall quality of the "microbead population" can be drawn.

In conclusion, the proposed method enables observation of catalytic polydispersity of immobilized enzymes – adding to the conventional bioanalytical toolkit used in biotechnology. Unlike a previously published method,[6] the current one enables temporal monitoring of transesterifications catalyzed by single microbeads, and there is no need that the product absorbs ultraviolet (UV) light. Thus, it can be noticed that the analytical approach presented in this work is different than many conventional assays. The current method targets transesterification activity of relatively small samples of heterogeneous biocatalysts (microbeads < 1 mm). Standard methods often target larger samples, focus on homogeneous catalysis, or probe hydrolytic activity (as opposed to transesterification activity of lipase). While GC-MS is an established analytical platform, the current method enables convenient coupling of the GC-MS instrument with a reaction system. Nonetheless, it should also be pointed out that the use of GC-MS apparatus – as opposed to the use of UV-Vis spectrophotometer – makes the overall cost of the current method higher. However, the automated system proposed here does not add much to the cost of the existing GC-MS instruments because the sampling device (**Figures 3.1** and **3.2**) has been constructed using inexpensive parts. It is estimated that the capital cost of the proposed sampling technology is ~ 10× lower than the cost of a commercial autosampler. Near-infrared spectroscopy is yet another technique for real-time monitoring of transesterifications.[102, 103] It is envisaged that

these optical methods – along with the "automated-sampling GC-MS approach" – will form a part of modern analytical toolkit for biocatalyst screening.

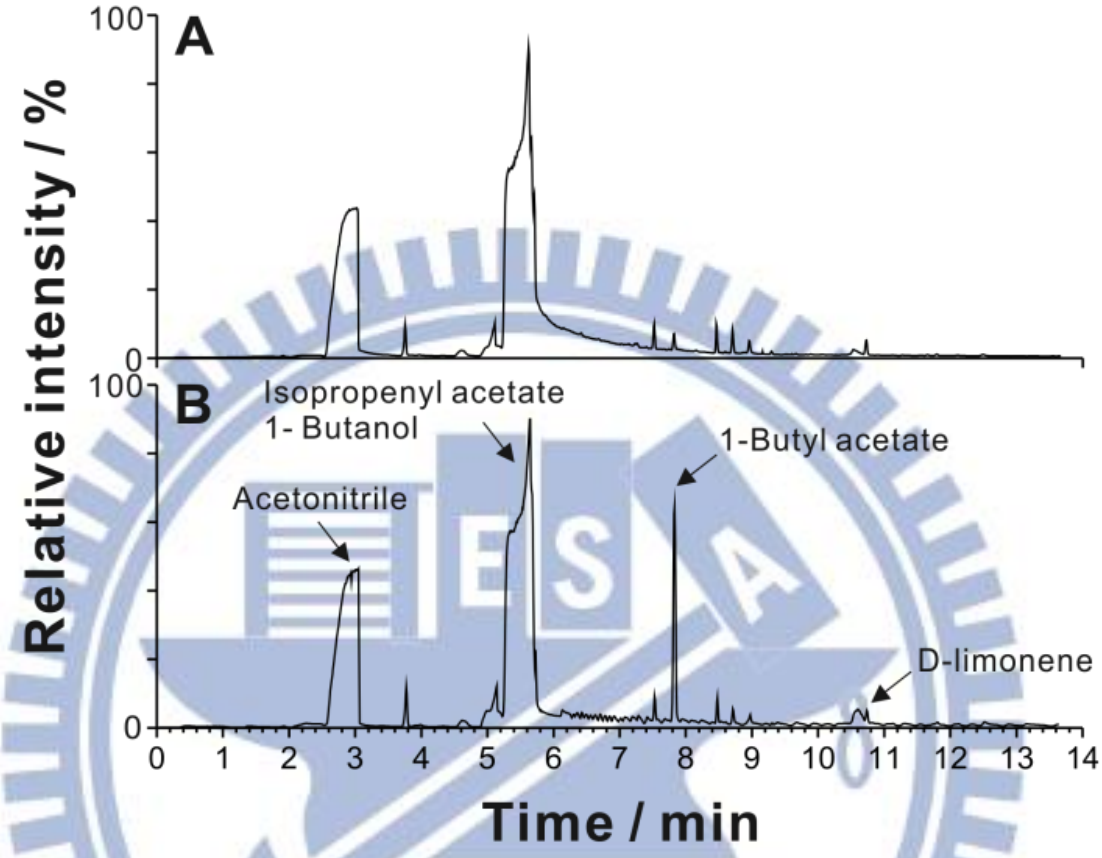

Figure 3.7 Full range GC-MS chromatograms (total ion currents, TICs, *m/z* range: 42-250 u e^{-1}) of the reaction (*cf.* eq. 3.1) mixture (5 mL; acetonitrile : 1-butanol : isopropenyl acetate = 90 : 9 : 1 (v/v/v)). (A) Blank containing the internal standard (no microbeads added). (B) Sample after 126-min incubation using 10 microbeads of lipase (see section **3.2.1.**). Temperature: 30 °C. Shaking speed: 20 rpm. The peak of the reaction product (1-butyl acetate) can be seen in (B). Internal standard: 10^{-5} M D-limonene.

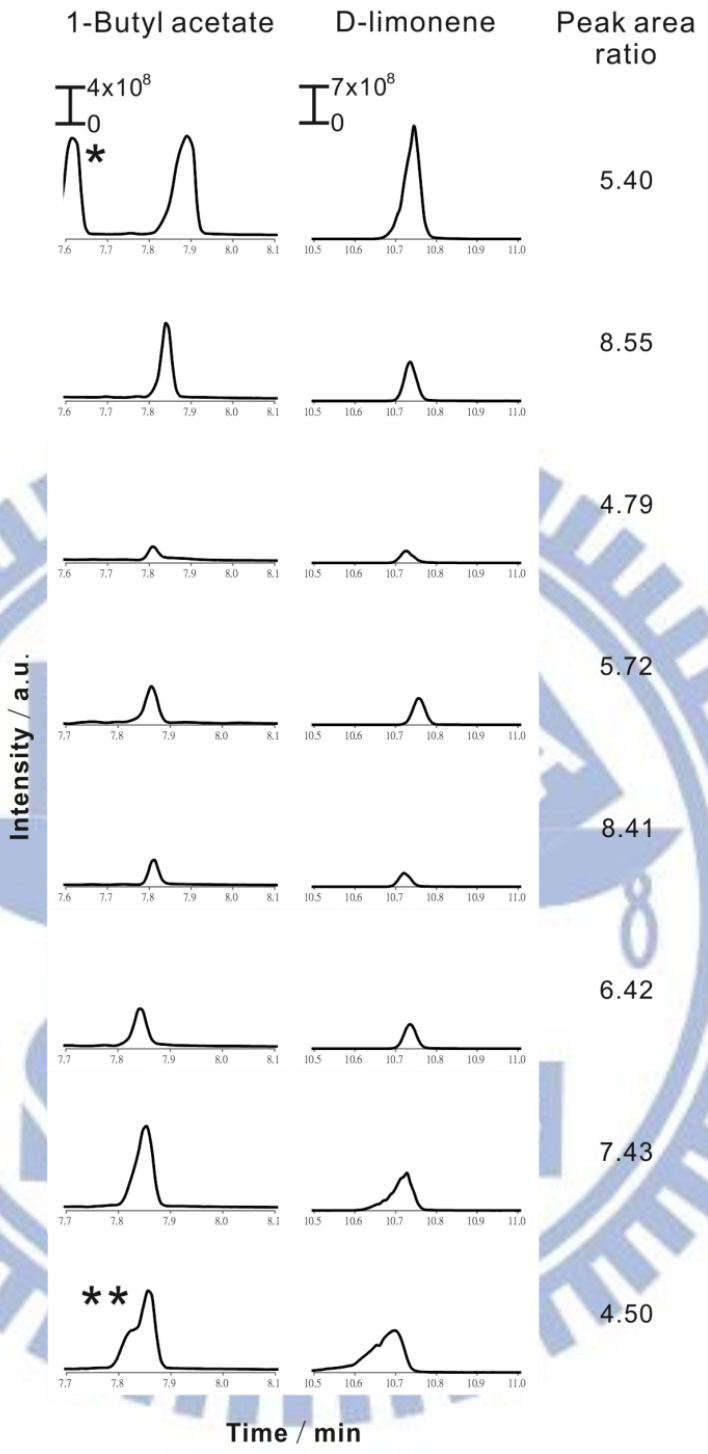

Figure 3.8 Raw EICs (analyte *m/z* 43 ± 0.5 u e^{-1}, internal standard *m/z*, 93 ± 0.5 u e^{-1}) for the data in **Figure 3.10** (analyses at 126 min). Conditions are the same as in **Figure 3.7**. Asterisk (*) indicates a contaminant peak which has a longer retention time when the amount of the reaction product is higher than usual. Two asterisks (**) indicate a fronting feature which is most probably related to an injection artifact.

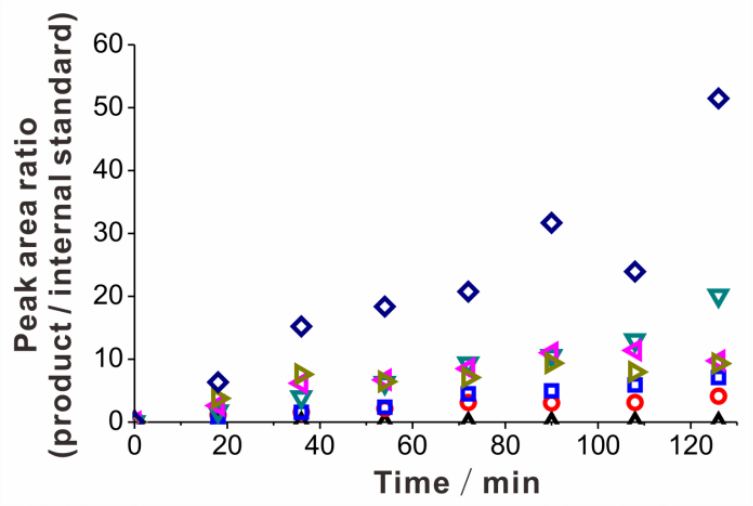

Figure 3.9 Synthesis of 1-butyl acetate catalyzed by small number of macroporous resin microbeads with immobilized lipase (from *Candida antarctica*; expressed in *Aspergillus oryzae*) monitored by the setup shown in **Figures 3.1** and **3.2**. Size range of microbeads: ~ 400-600 μm. Markers: (△, black triangle) 0 microbeads; (○, red circle) 1 microbead; (□, blue square) 2 microbeads; (▷, green tilted triangle) 3 microbeads; (▽, green reversed triangle) 4 microbeads; (◁, violet tilted triangle) 5 microbeads; (◇, dark blue diamond) 10 microbeads. Conditions are the same as in **Figure 3.7**. All the data point had been subtracted with the peak area ratio value at time "zero".

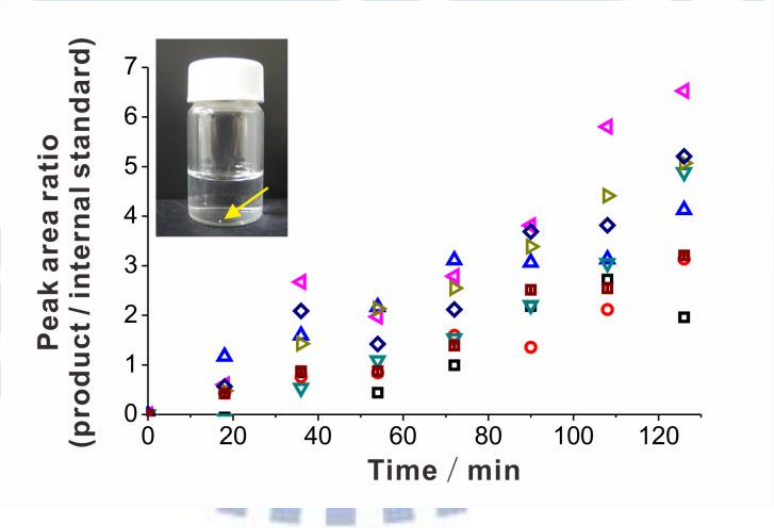

Figure 3.10 Single-microbead biocatalysis. Each curve corresponds to one lipase microbead. For EICs (analyte *m/z* 43 ± 0.5 u e^{-1}, internal standard *m/z* 93 ± 0.5 u e^{-1}) of the analyses at 126 min, see **Figure 3.8**. For the calculated reaction rates, see **Table 3.2**. Conditions are the same as in **Figure 3.7**. All the data points had been subtracted with the peak area ratio value at time "zero". The data marked with red circles (○, red circle) correspond to the same experiment as the one depicted in **Figure 3.9**. The inset shows the sample vial with a reaction mixture and one lipase microbead (indicated with yellow arrow).

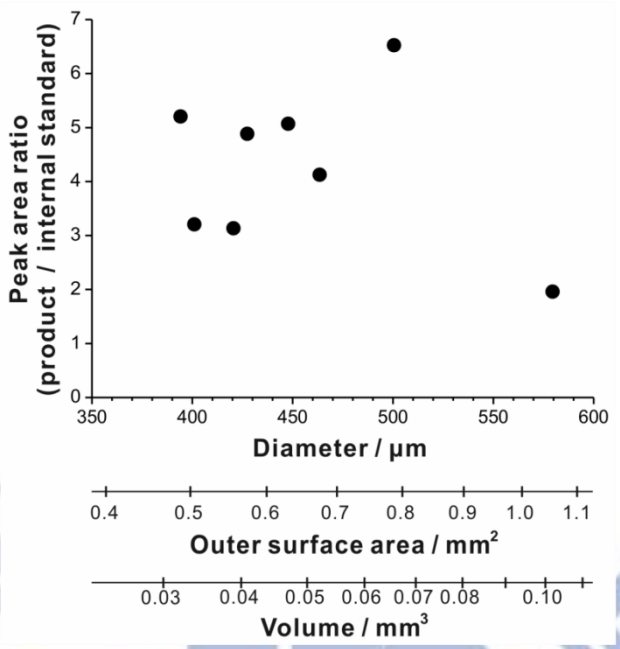

Figure 3.11 Dependence of the relative yield of the enzymatic reaction (after 126 min) on physical dimensions (diameter, outer surface area, volume) of the analyzed lipase microbeads according to the results of single-microbead assay (**Figures 3.8** and **3.10**). Peak areas were measured based on the EICs (analyte *m/z* 43 ± 0.5 u e^{-1}, internal standard *m/z*, 93 ± 0.5 u e^{-1}).

Table 3.3 Calculation of the lipase-catalyzed transesterification velocities obtained during the single-microbead transesterification experiment (**Figure 3.10**) facilitated by the proposed automated system (**Figures 3.1** and **3.2**).

Microbead symbol (*cf.* Figure 3.10)	**Fitted line *A* – area ratio *t* – time / min**	**Reaction velocity / nmol L^{-1} min^{-1}**
1, □	$A = (0.0190 \pm 0.0022)t$	308
2, ○	$A = (0.0208 \pm 0.0014)t$	315
3, □	$A = (0.0241 \pm 0.0012)t$	329
4, ▽	$A = (0.0293 \pm 0.0030)t$	351
5, ▷	$A = (0.0392 \pm 0.0007)t$	392
6, △	$A = (0.0343 \pm 0.0020)t$	372
7, ◇	$A = (0.0378 \pm 0.0023)t$	386
8, ◁	$A = (0.0487 \pm 0.0029)t$	432

3.3.4. Application in time-resolved extraction of plant tissue samples

To further demonstrate the capabilities of the proposed automated sampling system, we applied it in time-resolved monitoring of the extraction of a real sample (fresh peel of citrus fruit). In this experiment, the sample vial was filled with 5 mL of pure acetonitrile, incubated at 25 °C, and shaken. At time "zero", a small fragment of freshly obtained fruit peel was inserted to the vial, and the monitoring started. As the chromatograms were recorded, the increasing signals of certain plant metabolites could readily be observed. For example, the on-line extraction of lemon peel led to the emergence of several signals, including those identified as limonene, pinene and terpinene (**Figures 3.12** and **3.13**), which are abundant ingredients of citrus fruit.[104, 105] In the case of lemon, the signals of the three identified metabolites became strong after ~ 30 min extraction, and they were constant till the end of the experiment (**Figure 3.12A**). In the case of the kumquat sample, a substantial amount of limonene was extracted immediately on contact with extractant (**Figure 3.12B**). The time-resolved extraction profiles provide information on the availability of target analytes for extraction. In fact, a previous study – conducted in this laboratory (*N.B.* also utilizing universal electronic modules) – clearly demonstrated the usefulness of time-resolved extraction monitoring to reveal extractability of sample/specimen constituents.[106] Although no generalizations can be made based on the limited number of real samples, the current result proves that the method can reveal differences in extractability of selected plant tissue specimens. The extraction monitoring in real time – enabled by the proposed analytical system – can further facilitate optimization of extraction conditions by reducing the number of manual operations to minimum.

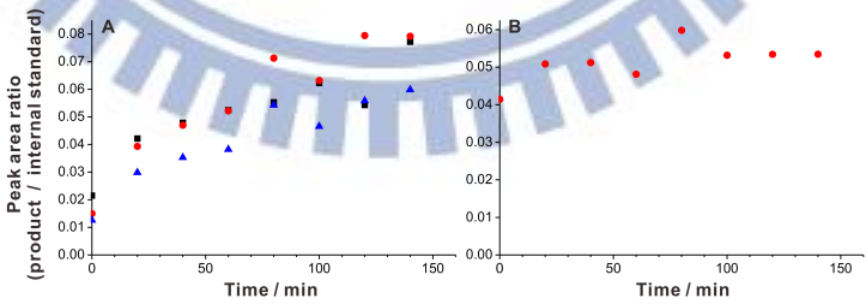

Figure 3.12 Monitoring extraction of real samples in real time. Time evolution of the extraction profiles. Extraction solvent: 5 mL acetonitrile. Temperature: 25 °C. Shaking speed: 20 rpm. Internal standard: 10^{-5} M thymol. (A) Lemon peel (m = 3.81 mg): (●) limonene, (■) pinene, (▲) terpinene. (B) Kumquat peel (m = 4.00 mg): (●) limonene. The analyses were conducted in duplicate and representative results are displayed.

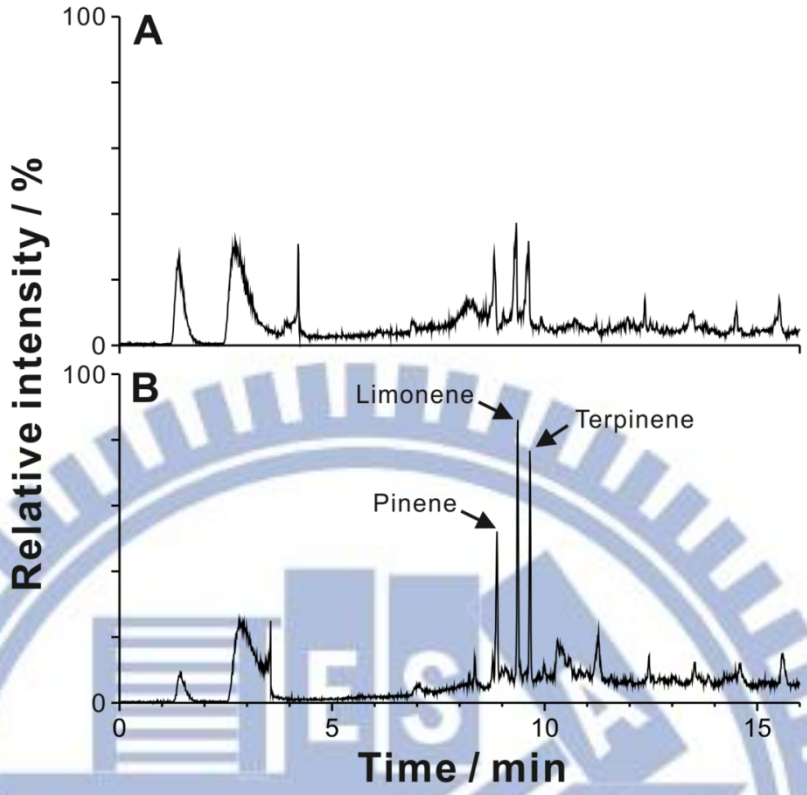

Figure 3.13 Monitoring extraction of the lemon peel sample in real time. Extraction solvent: 5 mL acetonitrile. Temperature: 298 K. Shaking speed: 20 rpm. Internal standard: 10^{-5} M thymol. (A) EIC at *m/z* 93 ± 0.5 u e^{-1} obtained at time "zero" (right after inserting the sample to the extraction solvent), and (B) EIC at *m/z* 93 ± 0.5 u e^{-1} obtained at a later stage of extraction (140 min). These mass spectra are from the same experiment as the one illustrated in **Figure 3.12A**.

3.4. Summary

We have demonstrated a simple device for automated sampling of dynamic chemical processes, and instantaneous analysis by GC-MS. The device coupled with a GC-MS apparatus is easy to use. It also offers the advantage of reducing the extent of mechanical operations during sampling and analysis. As exemplified in this report, it enables analyses of dynamic processes such as enzymatic reaction and extraction. The optimum conditions for these processes (*e.g.* temperature, shaking) can readily be achieved and maintained. One disadvantage of using this system is that the septum of the injector has to be replaced often in order to prevent leakage of the carrier gas. This problem can readily be rectified by substituting septum with a metal plate to which the needle of the injection system could be soldered permanently. Another consideration is that the current setup is mainly applicable to

short term monitoring since a few hundred microliters are withdrawn from the sample chamber – depleting the medium of reaction or extraction. This issue can be mitigated by using larger volumes of reaction/extraction solvents, in which case the depletion of solvent during sampling would only have negligible effect on the analysis result. To further improve the quantitative aspects of the presented method, it is suggested that isotopically labeled internal standards are used as additives to the reaction or extraction mixtures. Nonetheless, when doing so, attention must be paid so as to avoid experimental artifacts (by possible shifting of the reaction/extraction equilibria). Overall, we envisage that the proposed system can further be used for monitoring, optimization, and mechanistic studies on other chemical and biochemical processes. Following additional alterations to the valve unit assembly and the program, one might also consider coupling this system with other types of analytical instruments (for example, mass spectrometers, without separation systems), which would increase the range of potential applications. It is also interesting to note that – in this study – we have demonstrated the usefulness of a popular microcomputer (Raspberry Pi) in the construction of automated analytical systems, thus expanding the application realm of universal electronic modules in chemistry laboratories. Down this path, we believe that such miniature electronic systems will soon become an indispensable component of the instrumental tacklebox in chemistry, enticing industrious analysts into development of automated systems for a wide range of analytical tasks.

Chapter 4.

Summary and conclusions

In the two studies described above, mass spectrometry-based methods have been developed and used in the enzymatic reaction monitoring.

In the first study (Chapter 2), an atmospheric pressure ionization mass spectrometric method was implemented in the analysis of a bienzymatic reaction in a high aspect ratio cell. Using this simple analysis system, we demonstrated chemical signal transduction due to the progress of the enzymatic reaction in real time. The non-labelled and isotopically labeled ATP was used to trigger the reaction. This allowed us to disentangle the contributions of passive and active transport. The use of isotopic label helped to overcome the repeatability problems associated with experimental instabilities. The results shown in this thesis may give the aspect of mimicking the signal transduction triggered by ATP in model reaction and observe the behavior of bioautocatalytic reaction processes. also, others enzyme catalyzed reaction can be monitoring by this method.

In the second study (Chapter 3), we developed an automated injection system for sampling and temporal analysis of dynamic samples. In this system, all the electronic elements were controlled by the Raspberry Pi microcomputer programmed in C language. The system automatically withdrew aliquots of samples from the vial (*e.g.* reaction chamber) and transferred them to the injection port of a GC-MS apparatus. Transesterification was selected as a model of enzymatic reaction to demonstrate the capabilities of the proposed approach. The reaction was catalyzed by immobilized lipase beads. For the first time, we demonstrated the ability to monitor transesterification reaction catalyzed by single beads of lipase. Catalytic heterogeneity of immobolized beads of lipase was revealed. The interesting thing is that catalytic activities of lipase beads and beads size are not correlated. It shows that the immobilized lipase biocatalyst is not uniform. Furthermore, using this system, we demonstrated real-time monitoring of extraction of biological samples. Terpenes from plant tissue sample were identified. Quantitative analysis of of transesterification of product and the extracted terpene species were accomplished. We expect that this automated system can be further used not only in enzyme assay, but also in other applications. For example, it may potentially be used to monitor wastewater discharge by factory, and evaluate the level of pollutants or toxic substances in the environment.

Appendix

Permission for **Figure 1.3** (reproduced from ref.[28])

RightsLink

WILEY

Book: Modern Practice of Gas Chromatography, 4th Edition
Author: Robert L. Grob, PhD (Editor), Eugene F. Barry, PhD (Editor)
Publisher: John Wiley and Sons
Date: May 1, 2004
Copyright © 2004, John Wiley and Sons

Logged in as: Hsu Ting
Account #: 3000799743

Order Completed

Thank you very much for your order.

This is a License Agreement between Hsu Ting ("You") and John Wiley and Sons ("John Wiley and Sons"). The license consists of your order details, the terms and conditions provided by John Wiley and Sons, and the payment terms and conditions.

Get the printable license.

License Number	3435420825700
License date	Jul 24, 2014
Licensed content publisher	John Wiley and Sons
Licensed content publication	Wiley Books
Licensed content title	Modern Practice of Gas Chromatography, 4th Edition
Book title	Modern Practice of Gas Chromatography, 4th Edition
Licensed copyright line	Copyright © 2004, John Wiley and Sons
Licensed content author	Robert L. Grob, PhD (Editor), Eugene F. Barry, PhD (Editor)
Licensed content date	May 1, 2004
Type of use	Dissertation/Thesis
Requestor type	University/Academic
Format	Print and electronic
Portion	Figure/table
Number of figures/tables	2
Original Wiley figure/table number(s)	Figure 3.27
Will you be translating?	No
Title of your thesis / dissertation	Development of Mass Spectrometric Methods for the Monitoring of Biocatalytic Processes
Expected completion date	Jul 2014
Expected size (number of pages)	72
Total	0.00 USD

ORDER MORE... CLOSE WINDOW

Copyright © 2014 Copyright Clearance Center, Inc. All Rights Reserved.
Privacy statement.
Comments? We would like to hear from you. E-mail us at customercare@copyright.com

Permission for **Figure 1.7** (reproduced from ref.[41])

Licensed content publisher	John Wiley and Sons
Licensed content publication	Journal of Mass Spectrometry
Licensed content title	Electrospray: Principles and Practice
Licensed copyright line	Copyright © 1997 John Wiley & Sons, Ltd.
Licensed content author	Simon J. Gaskell
Licensed content date	Dec 4, 1998
Start page	677
End page	688
Type of use	Dissertation/Thesis
Requestor type	University/Academic
Format	Print and electronic
Portion	Figure/table
Number of figures/tables	1
Original Wiley figure/table number(s)	Fugure 1
Will you be translating?	No
Title of your thesis / dissertation	Development of Mass Spectrometric Methods for the Monitoring of Biocatalytic Processes
Expected completion date	Jul 2014
Expected size (number of pages)	72
Total	0.00 USD

ORDER MORE... CLOSE WINDOW

Copyright © 2014 Copyright Clearance Center, Inc. All Rights Reserved.
Privacy statement.
Comments? We would like to hear from you. E-mail us at

References

1. Naturhistorisch-medizinischen Verein, H., Verhandlungen des Naturhistorisch-medizinischen Vereins zu Heidelberg. Heidelberg, Selbtsverlag: **1877**; 190.
2. Buchner, E., Cell-free fermentation. Nobel Lecture, **1907**.
3. Sumner, J. B., The chemical nature of enzymes. Nobel Lecture, **1946**.
4. Olempska-Beer, Z. S.; Merker, R. I.; Ditto, M. D.; DiNovi, M. J., *Regul. Toxicol. Pharm.*, **2006**, 45, 144-158.
5. Pundir, C. S.; Chauhan, N., *Ind. Eng. Chem. Res.*, **2012**, 51, 3556-3563.
6. Bajpai, P., *Biotechnol. Prog.*, **1999**, 15, 147-157.
7. Araujo, R.; Casal, M.; Cavaco-Paulo, A., *Biocatal. Biotransform.*, **2008**, 26, 332-349.
8. Rottig, A.; Wenning, L.; Broker, D.; Steinbuchel, A., *Appl. Microbiol. Biotechnol.*, **2010**, 85, 1713-1733.
9. Jegannathan, K. R.; Nielsen, P. H., *J. Clean. Prod.*, **2013**, 42, 228-240.
10. Nelson, D. L. C. M. M., *Lehninger principles of biochemistry*. 3 rd ed.; Worth: New York, **2000**.
11. Zhou, J. W.; Liu, L. M.; Shi, Z. P.; Du, G. C.; Chen, J., *Biotechnol. Adv.*, **2009**, 27, 94-101.
12. Gordon, A. M.; Homsher, E.; Regnier, M., *Physiol. Rev.*, **2000**, 80, 853-924.
13. Johnson, A.; O'Donnell, M., *Annu. Rev. Biochem.*, **2005**, 74, 283-315.
14. Del Favero, M.; Mazzantini, E.; Briani, F.; Zangrossi, S.; Tortora, P.; Deho, G., *J. Biol. Chem.*, **2008**, 283, 27355-27359.
15. Schoffelen, S.; van Hest, J. C. M., *Soft Matter*, **2012**, 8, 1736-1746.
16. Meher, L. C.; Sagar, D. V.; Naik, S. N., *Renew. Sust. Energ. Rev.*, **2006**, 10, 248-268.
17. Thakur, S., *IJSER*, **2012**, 3, 1-29.
18. Ettre, L. S., *Chromatographia*, **2000**, 51, 7-17.
19. Bard A. J., Faulkner L. R., *Electrochemical Methods: Fundamentals and Applications*. 2 ed.; Wiley: **2001**.
20. Tkachenko, N., *Optical Spectroscopy, Methods and Instrumentations*. 1 ed.; Elsevier.
21. Cooks, R. G.; Busch, K. L.; Glish, G. L., *Science*, **1983**, 222, 273-291.
22. Skoog, D. A. W., D. M.; Holler, F. J.; Crouch S. R. , *Fundamentals of Analytical Chemistry*. 8 th ed.; Brooks/Cole: Belmont., **2004**.

23. Tswett, M. S., *Proceedings of the Warsaw Society of Naturalists*, **1903**, 14, 20-39.
24. Pourmortazavi, S. M.; Rahimi-Nasrabadi, M.; Hajimirsadeghi, S. S., *Curr. Anal. Chem.*, **2014**, 10, 3-28.
25. Martin, A. J. P.; Synge, R. L. M., *Biochem. J.*, **1941**, 35, 1358-1368.
26. Hawkes, S. J., *J. Chem. Educ.*, **1983**, 60, 393-398.
27. James, A. T.; Martin, A. J. P., *Biochem. J.*, **1952**, 50, 679-690.
28. Grob, R. L.; Barry, E. F., *Modern Practice of Gas Chromatography*. 4th ed.; Wiley: Hoboken, **2004**.
29. de Zeeuv, J.; Luong, J., *Trends Anal. Chem.*, **2002**, 21, 594-607.
30. Muller, R. K.; Grosse, J.; Thieme, D.; Lang, R.; Teske, J.; Trauer, H., *J. Chromatogr. A*, **1999**, 843, 275-285.
31. Santos, F. J.; Galceran, M. T., *Trends Anal. Chem.*, **2002**, 21, 672-685.
32. Lehotay, S. J.; Hajslova, J., *Trends Anal. Chem.*, **2002**, 21, 686-697.
33. Challinor, J. M., *Forensic Sci. Int.*, **1983**, 21, 269-285.
34. Lu, Y.; Harrington, P. B., *Anal. Chem.*, **2007**, 79, 6752-6759.
35. Collin, O. L.; Niegel, C.; DeRhodes, K. E.; McCord, B. R.; Jackson, G. P., *J. Forensic Sci.*, **2006**, 51, 815-818.
36. Kováts, E., *Helv. Chim. Acta.*, **1958**, 41, 1915.
37. Williamson, L. N.; Bartlett, M. G., *Biomed. Chromatogr.*, **2007**, 21, 664-669.
38. Fenn, J. B.; Mann, M.; Meng, C. K.; Wong, S. F.; Whitehouse, C. M., *Science*, **1989**, 246, 64-71.
39. Fenn, J. B., *Electrospray wings for molecular elephants*, Nobel Lecture, **2002**.
40. Robinson, C. V., *FEBS J.*, **2012**, 279, 663-677.
41. Gaskell, S. J., *J. Mass Spectrom.*, **1997**, 32, 677-688.
42. Bruins, A. P., *J. Chromatogr. A*, **1998**, 794, 345-357.
43. Cech, N. B.; Enke, C. G., *Mass Spectrom. Rev.*, **2001**, 20, 362-387.
44. Takats, Z.; Wiseman, J. M.; Gologan, B.; Cooks, R. G., *Science*, **2004**, 306, 471-473.
45. Cody, R. B.; Laramee, J. A.; Durst, H. D., *Anal. Chem.*, **2005**, 77, 2297-2302.
46. Shiea, J.; Huang, M. Z.; HSu, H. J.; Lee, C. Y.; Yuan, C. H.; Beech, I.; Sunner, J., *Rapid Commun. Mass Spectrom.*, **2005**, 19, 3701-3704.
47. Santos, V. G.; Regiani, T.; Dias, F. F. G.; Romao, W.; Jara, J. L. P.; Klitzke, C. F.; Coelho, F.; Eberlins, M. N., *Anal. Chem.*, **2011**, 83, 1375-1380.
48. Geankoplis, C. J., *Transport Processes and Unit Operations*. 3rd ed.; Prentice-Hall: Englewood Cliffs, N.J., **1993**.

49. Wolfgang Paul, H. S., *Z. Naturforsch.*, **1953**, 8A, 448.
50. March, R. E., *J. Mass Spectrom.*, **1997**, 32, 351-369.
51. Louris, J. N.; Cooks, R. G.; Syka, J. E. P.; Kelley, P. E.; Stafford, G. C.; Todd, J. F. J., *Anal. Chem.*, **1987**, 59, 1677-1685.
52. Safranyos, R. G. A.; Caveney, S., *J. Cell Biol.*, **1985**, 100, 736-747.
53. Shafrir, Y.; ben-Avraham, D.; Forgacs, G., *J. Cell Sci.*, **2000**, 113, 2747-2757.
54. Wang, F.; Wang, H.; Wang, J.; Wang, H. Y.; Rummel, P. L.; Garimella, S. V.; Lu, C., *Biotechnol. Bioeng.*, **2008**, 100, 150-158.
55. Chen, C. H. S., J. G., *J. Microelectromech. Syst.*, **2002**, 11, 672.
56. Kolmogorov A., P. I., Piskunov N., *Moscow Bull. Univ. Math.*, **1937**, 1, 1.
57. Fisher, R. A., *Ann. Eugenics*, **1937**, 7, 355.
58. Almarcha, C.; Trevelyan, P. M. J.; Grosfils, P.; De Wit, A., *Phys. Rev. Lett.*, **2010**, 104.
59. Valero, E.; Varon, R.; Garcia-Carmona, F., *Biochem. J.*, **2000**, 350, 237-243.
60. Urban, P. L.; Amantonico, A.; Fagerer, S. R.; Gehrig, P.; Zenobi, R., *Chem. Commun.*, **2010**, 46, 2212-2214.
61. Chen, Y. C.; Urban, P. L., *Trends Anal. Chem.*, **2013**, 44, 106-120.
62. Zaikin, A. N.; Zhabotinsky, A. M., *Nature*, **1970**, 225, 535-537.
63. Saiki, R. K.; Scharf, S.; Faloona, F.; Mullis, K. B.; Horn, G. T.; Erlich, H. A.; Arnheim, N., *Science*, **1985**, 230, 1350-1354.
64. Li, P. H.; Ting, H.; Chen, Y. C.; Urban, P. L., *RSC Adv.*, **2012**, 2, 12431-12437.
65. Winfree, A. T., *The Geometry of Biological Time*. Springer: Verlag, New York, **2010**.
66. Chen, X.; Briggs, N.; McLain, J. R.; Ellington, A. D., *Proc. Natl. Acad. Sci. USA*, **2013**, 110, 5386-5391.
67. Goddard, J. P.; Reymond, J. L., *Curr. Opin. Biotechnol.*, **2004**, 15, 314-322.
68. Min, D. H.; Tang, W. J.; Mrksich, M., *Nat. Biotechnol.*, **2004**, 22, 717-723.
69. Reymond, J. L., *Food Technol. Biotech.*, **2004**, 42, 265-269.
70. Slade, R. E.; Pauling L. C., *Weekly Evening Meeting, London, 27 Feb; Royal Institution of Great Britain*: London, **1948**.
71. Marti, S.; Roca, M.; Andres, J.; Moliner, V.; Silla, E.; Tunon, I.; Bertran, J., *Chem. Soc. Rev.*, **2004**, 33, 98-107.
72. Urban, P. L.; Goodall, D. M.; Bergstrom, E. T.; Bruce, N. C., *J. Biotechnol.*, **2006**, 126, 508-518.
73. Skoog, D. A.; Holler, F. J.; Crouch, S. R., *Principles of Instrumental Analysis*. 6 th ed.; Brooks/Cole: Belmont, **2007**.

74. Helmig, D., *J. Chromatogr. A*, **1999**, 843, 129-146.
75. Papoutsis, I. I.; Athanaselis, S. A.; Nikolaou, P. D.; Pistos, C. M.; Spiliopoulou, C. A.; Maravelias, C. P., *J. Pharmaceut. Biomed.*, **2010**, 52, 609-614.
76. Fan, X.; Wei, X. Y.; Zong, Z. M., *Fuel*, **2013**, 109, 28-32.
77. Marriott, P. J.; Shellie, R.; Cornwell, C., *J. Chromatogr. A*, **2001**, 936, 1-22.
78. Koek, M. M.; Bakels, F.; Engel, W.; van den Maagdenberg, A.; Ferrari, M. D.; Coulier, L.; Hankemeier, T., *Anal. Chem.*, **2010**, 82, 156-162.
79. Thermo Scientific, TriPlus RSH Autosampler, Integrated Sampling System, Brochure. Waltham, MA, USA, 2011–2012; p BR52235_E 09/12M.
80. Reina, E.; Camacho, L.; Casas, J.; Van Veldhoven, P. P.; Fabrias, G., *Chem. Phys. Lipids*, **2012**, 165, 225-231.
81. Ghanem, A.; Schurig, V., *Chirality*, **2000**, 13, 118-123.
82. Kulkarni, N.; Gadre, R. V., *Biotechnol. Tech.*, **1998**, 12, 627-628.
83. Avdikos, E. M.; Prodromidis, M. I.; Efstathiou, C. E., *Sens. Actuat. B*, **2005**, 107, 372-378.
84. Singh, R. M. M., R.; Ahemad R. , *Int. J. Eng. Innov. Technol*, **2012**, 2, 70-73.
85. Raspberry Pi website, http://www.raspberrypi.org/ (viewed on 03/03/2014).
86. BBC News Technology, http://www.bbc.co.uk/news/technology-17190918 (viewed on 03/03/2014).
87. Upton, E., *Computer*, **2013**, 46, 14-16.
88. TechRepublic, http://www.techrepublic.com/blog/european-technology/10-coolest-uses-for-the-raspberry-pi/505/#. (viewed on 03/03/2014).
89. DesignSpark, http://www.designspark.com/blog/ten-essential-raspberry-pi-projects (viewed on 03/03/2014).
90. Arduino website, http://arduino.cc/ (viewed on 03/03/2014).
91. Netduino website, http://netduino.com/ (viewed on 03/03/2014).
92. mbed website, https://mbed.org/ (viewed on 03/03/2014).
93. BeagleBoard website, http://beagleboard.org/Products/BeagleBone/ (viewed on 03/03/2014).
94. Pearce, J. M., *Science*, **2012**, 337, 1303-1304.
95. Pearce, J. M., *Nature*, **2014**, 505, 618-618.
96. Open-source Lab, http://www.appropedia.org/Open-source_Lab#Open-Source_Lab.2C_1st_Edition:_How

_to_Build_Your_Own_Hardware_and_Reduce_Research_Costs/ (viewed on 03/03/2014).

97. Quintana, J. B.; Boonjob, W.; Miro, M.; Cerda, V., *Anal. Chem.*, **2009**, 81, 4822-4830.
98. Clavijo, S.; Fernandez, M.; Forteza, R.; Brunetto, M. D.; Cerda, V., *Anal. Meth.*, **2014**, 6, 3335-3344.
99. Goujard, L.; Villeneuve, P.; Barea, B.; Lecomte, J.; Pina, M.; Claude, S.; Le Petit, J.; Ferre, E., *Anal. Biochem.*, **2009**, 385, 161-167.
100. Gilham, D.; Lehner, R., *Methods*, **2005**, 36, 139-147.
101. Konarzycka-Bessler, M.; Bornscheuer, U. T., *Angew. Chem. Int. Ed.*, **2003**, 42, 1418-1420.
102. Arias, E. L. M.; Martins, P. F.; Munhoz, A. L. J.; Gutierrez-Rivera, L.; Maciel, R., *Ind. Eng. Chem. Res.*, **2012**, 51, 10755-10767.
103. Zhang, F.; Adachi, D.; Tamalampudi, S.; Kondo, A.; Tominaga, K., *Energ. Fuel*, **2013**, 27, 5957-5961.
104. Ahmad, M. M.; Salim Ur, R.; Iqbal, Z.; Anjum, F. M.; Sultan, J. I., *Pak. J. Bot.*, **2006**, 38, 319-324.
105. Bourgou, S.; Rahali, F. Z.; Ourghemmi, I.; Tounsi, M. S., *Sci. World J.*, **2012**, 2012, 1-12.
106. Hu, J. B.; Chen, S. Y.; Wu, J. T.; Chen, Y. C.; Urban, P. L., *RSC Adv.*, **2014**, 4, 10693-10701.